2020

Transcatheter Mitral Valve Replacement: Structural and Hemodynamic Analysis

Saba Ravaghi

Transcatheter Mitral Valve Replacement: Structural and Hemodynamic Analysis

A Thesis

Presented to

the Faculty of the Daniel Felix Ritchie School of Engineering and Computer Science

University of Denver

In Partial Fulfillment

of the Requirements for the Degree

Master of Science

by

Saba Ravaghi

June 2020

Advisor: Dr. Ali N. Azadani

Author: Saba Ravaghi
Title: Transcatheter Mitral Valve Replacement: Structural and Hemodynamic Analysis
Advisor: Dr. Ali N. Azadani
Degree Date: June 2020

ABSTRACT

Transcatheter mitral valve replacement (TMVR) is being developed to become a substitute therapy for surgery in prohibitive or high surgical risk patients to treat severe mitral regurgitation. A limited number of TMVR systems are under clinical evaluation. However, transcatheter mitral valve (TMV) long-term durability and hemodynamic performance is not known. TMV durability and hemodynamics must match with that of surgical bioprostheses for potential commercialization of TMVR. Experimental and computational approaches were used to find the leaflets' three-dimensional anisotropic mechanical properties in a transcatheter Edwards SAPIEN 3 valve and a surgical Carpentier-Edwards PERIMOUNT Magna mitral valve and finite element (FE) simulations were conducted to obtain the stress distribution on both valves. Moreover, to visualize the flow field within the left heart, steady-state computational fluid dynamics (CFD) simulations were run. The FE simulations demonstrated that in a cardiac cycle, at peak systole, the highest stress value in the two bioprostheses was 4.75 and 16 MPa for the surgical and transcatheter heart valve, respectively. After studying the leaflet stress distributions and flow field, long-term durability may potentially be different between the two models. The results of CFD simulations could potentially show that TMVs with supra-annular positioning have a higher risk of leaflet thrombosis as opposed to the intra-annular position.

TABLE OF CONTENTS

LIST OF FIGURES

LIST OF ABBREVIATIONS

AVR	Aortic Valve Replacement
CABG	Coronary Artery Bypass Grafting
FDA	Food and Drug Administration
FMR	Functional Mitral Regurgitation
GDMT	Guideline-Directed Medical Therapy
LVEF	Left Ventricular Ejection Fraction
LVOT	Left Ventricular Outflow Tract
MR	Mitral Regurgitation
MVR	Mitral Valve Replacement
PVL	Paravalvular Leakage
SAV	Surgical Aortic Valve
SAVR	Surgical Aortic Valve Replacement
SVD	Structural valve Degeneration
TAV	Transcatheter Aortic Valve
TAVR	Transcatheter Aortic Valve Replacement
TEE	Transesophageal Echocardiography
THV	Transcatheter Heart Valve
TMVR	Transcatheter Mitral Valve Replacement
$TMVR_e$	Transcatheter Mitral Valve Repair
TViV	Transcatheter Valve-in-Valve

CHAPTER ONE: INTRODUCTION

Mitral regurgitation (MR) is a widespread valvular heart disease in the western world. In the United States alone, it is estimated that the prevalence of moderate and severe MR is between 2 to 2.5 million at present. This number is predicted to reach 5 million cases by 2030 (1). MR presence rises with age, resulting in a sharp increase in the number of patients in need of hospital care and intervention over the next decades (2). The consequences of untreated MR include progressive left ventricular (LV) dilation, myocardial dysfunction, and cardiac failure, resulting in considerable morbidity and mortality, and creating a great economic burden (3). MR is categorized into two types based on etiology: degenerative (primary) and functional (secondary).

Primary MR is defined as any abnormalities in the mitral valve apparatus that cause MR. The Carpentier classification is used to differentiate etiologies in MR (Figure 1). In Carpentier type I, MR is caused by a perforation in the leaflets or congenital clefts but the leaflets have normal size and motion. Flail leaflets or excessive leaflet motion with prolapse are categorized as Carpentier type II MR. Restricted leaflet motion during diastole is witnessed in Carpentier type IIIa MR. Contrary to primary MR, secondary MR has nothing to do with the mitral valve itself; a diseased left atrium or ventricle is causing the MR. Ischemic and nonischemic cardiomyopathy are two main types of ventricular disease that lead to MR. Due to nonischemic cardiomyopathy, annular dilation and loss of annular

contraction occurs, resulting in an increase of the effective regurgitation orifice (ERO) and MR. This is classified as Carpentier type I MR as the leaflets and their motion are normal, but the dilated annulus causes malcoaptation of the leaflets. Another Carpentier type I form of functional MR is the annular dilation secondary to severe left atrial enlargement. Ischemic cardiomyopathy however, results in Carpentier type IIIb (restricted leaflet motion during systole) MR as it introduces regional inferior ventricular wall motion abnormalities which in turn leads to tethered posterior leaflets and a posterior-oriented MR (2).

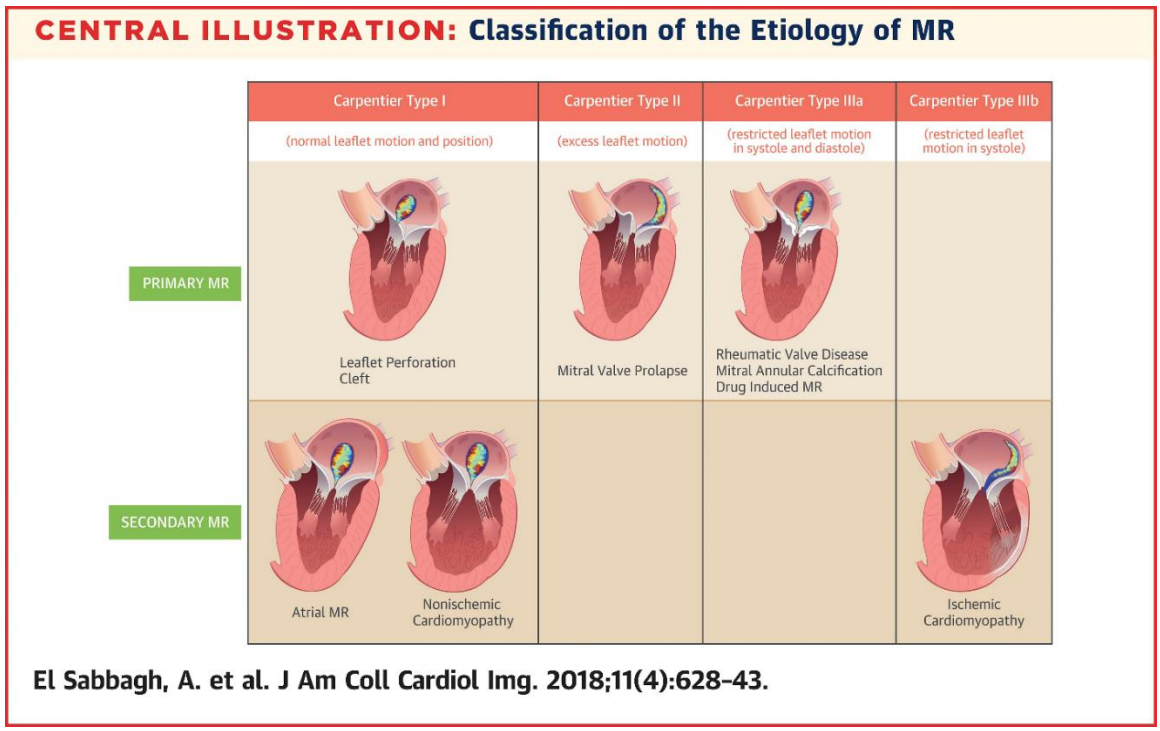

Figure 1-Classification of the etiology of MR with the Carpentier classification. Reprinted with permission from (2).

Currently, in symptomatic patients that present with chronic severe primary MR and left ventricular ejection fraction (LVEF) of greater than 30%, mitral valve surgery is recommended and may be considered with LVEF less than or equal to 30%. For asymptomatic patients with chronic severe primary MR, mitral valve surgery is

recommended when patient is presented with left ventricle (LV) dysfunction and is reasonable with preserved LV function. The treatment plan for chronic secondary MR is harder to define as MR is the aftermath of the main disease, therefore just restoring the mitral valve's capability is not curative. So in patients with chronic severe secondary MR, it is only deemed reasonable to do mitral valve surgery when patients are undergoing coronary artery bypass grafting (CABG) or aortic valve replacement (AVR) as well (4). In surgical MR treatment, repair and replacement are two available options although repair is generally favored over replacement (5)(6)(7).Surgical repair has led to favorable outcomes for the following diseases: annular dilation, degenerative mitral valve disease, leaflet perforation in endocarditis, chordal rupture, and ischemic papillary muscle dysfunction. Conversely, in elderly patients with rheumatic heart disease and calcified valves, or severe thickening of sub-valvular apparatus, outcomes are less favorable and surgical mitral replacement is the opted treatment plan (8).

The advantages of surgical repair over replacement for degenerative mitral valve disease have been confirmed by numerous studies and include: higher early and late survival rates, better preservation of left ventricular function, and elimination of complications related to a prosthetic valve replacement such as thromboembolism, anticoagulation medication and endocarditis (7). In terms of durability, retrospective data shows valve repair is as durable or even more durable than replacement, keeping in mind that standard comparisons are with durability of a mechanical valve replacement (6). A recent 20-year outcome study also concluded that in degenerative cases with flail leaflets, MV repair has lower operative mortality, superior long-term survival, and less valve-related complications compared with MV replacement. The study mentions changes in

surgical method for repair overtime but overall, any surgical method was complemented with a type of annuloplasty (5). It should be noted that a successful durable mitral repair is highly dependent on surgeon experience and is technically more complex than replacement (8).

For functional MR (FMR), the benefits of surgical repair over replacement are not as clear. In ischemic mitral regurgitation (IMR) cases, a systematic review concluded that literature shows repair might be result in better surgical mortality and long-term survival in comparison with replacement, but also expressed significant uncertainty in the conclusion due to the heterogeneity of the available studies (6). A prevalent repair option for functional MR cases is mitral annuloplasty (MAP); studies suggest low postoperative mortality, improved heart failure symptoms, positive changes in ventricle size and ejection fraction with good outcomes in the intermediate time frame (9). Commonly, undersized mitral annuloplasty is used as a simple and reproducible approach for chronic IMR patients with the justification that undersizing the mitral annulus ameliorates regurgitation through improving coaptation of the leaflets (10). However, five-year survival after annuloplasty in FMR patients is at the unsatisfactory rate of 50% (11) and recurrent MR of moderate or worse level was reported in 28% of patients at 6 months post-op (10). The efficacy of MAP in comparison with mitral valve replacement (MVR) for functional MR patients was investigated, concluding that subvalvular apparatus sparing MVR is a safe substitute for MAP which leads to noticeable reduction of MR severity and LV size. The study suggested that for patients with multiple comorbidities, severe tethering and complicated regurgitation jets, subvalvular apparatus sparing MVR should be considered (11).

However, most severe MR cases do not get referred for surgery due to the high risks associated with the patients' advanced age and various comorbidities, and the efficacy of valve surgery for secondary MR with LV dysfunction is still under question (3). In order to respond to the unmet clinical need of these MR cases, transcatheter mitral valve interventions have emerged as a minimally invasive, promising therapeutic substitute for surgery in inoperable or high-risk patients. Moreover, success of transcatheter aortic valve replacement (TAVR) over the last decade has motivated the drive for new transcatheter therapies targeted specifically to replace and repair the mitral valve. However, the engineering and clinical progress is slower than expected due to the challenges that come with the mitral valve such as the variety in etiology, the asymmetric and large mitral annulus, the dynamic environment of the LV and the critical outflow tract, necessity for complex and large delivery systems, and thromboembolism risk factors (12). These challenges will be covered more in depth further along in the text. Transcatheter repair and replacement are the two approaches that are either offered to patients or under investigation right now.

Percutaneous transcatheter mitral valve repair ($TMVR_e$) methods have been classified based on the specific anatomy that they target and are listed as follows:

1) Leaflets: Edge-to-edge MV repair, leaflet coaptation, leaflet ablation

2) Annulus: indirect annuloplasty through the coronary sinus or direct annuloplasty

3) Chordae: percutaneous chordal implantation

4) LV: percutaneous LV remodeling (1)

Currently, the MitraClip (Abbott, Chicago, IL, USA) device has the largest clinical experience with over 50,000 patients treated worldwide. It provides an edge-to-edge leaflet

repair and is the only transcatheter treatment for primary or secondary MR that is guideline recommended (12). The procedure is done under the guidance of transesophageal echocardiography (TEE) and fluoroscopy, going up the femoral vein and accessing the left atrium with an atrial-transseptal puncture. Entering inside the mitral valve (MV), the anterior and posterior leaflet free edges are grasped where there is malcoaptation and clipped together (13). The EVEREST II study (Endovascular Valve Edge-to Edge Repair) was a randomized trial of low-risk patients with primary or secondary MR and demonstrated that MitraClip is less effective, but safer than MV surgery, therefore receiving Food and Drug Administration (FDA) approval in the US for symptomatic patients with significant primary MR and at high surgical risk (14). But further evidence was required to approve the benefit of MitraClip in improving secondary MR. The COAPT trial was designed as a randomized study to evaluate effectiveness of MitraClip in treating clinically significant secondary MR in symptomatic heart failure patients who have been deemed as inappropriate for MV surgery. All patients were taking maximally tolerated guideline-directed medical therapy (GDMT). The study concluded that in the group that underwent transcatheter mitral valve repair as well as GDMT, at a 24 months of follow-up, lower hospitalization rate for heart failure, lower mortality, and better functional capacity and quality of life were observed compared to the group that just took medical therapy (15). The MitraClip delivery system and device are shown in Figure 2.

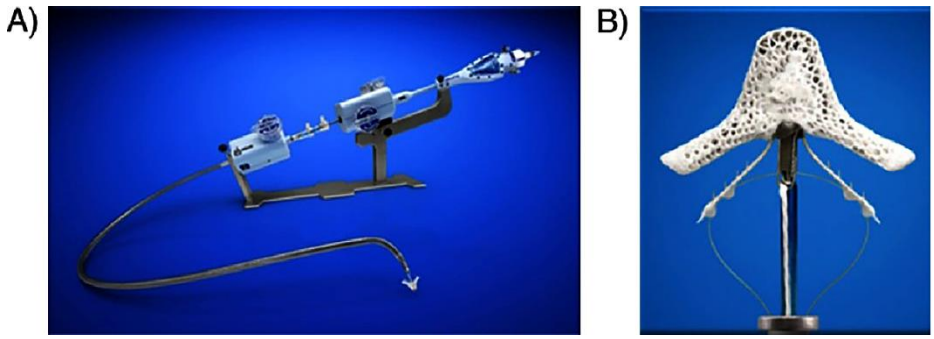

Figure 2-MitraClip a) delivery system b)clip itself. Reprinted with permission from (16).

Other percutaneous $TMVR_e$ technologies are based on the techniques used in chordal implantation and annuloplasty, and are still under development or in early clinical stages (1). These therapies try to mimic the techniques that surgical annuloplasty uses. Three catheter-based direct annuloplasty systems are undergoing early clinical studies: the Cardioband (Edwards Lifesciences, Irvine, CA), the Mitralign (Mitralign Inc., Tewksbury, Massachusetts) and the Accucinch (Guided Delivery Systems, Santa Clara, California) (17). Cardioband seems to be the furthest ahead in development, gaining CE-Mark in 2015 to treat severe FMR. This system is derived from the undersized ring in surgical repair and is fully percutaneous and adjustable while also allowing for other interventions on the leaflets. An image of the deployed device is shown in Figure 3. The Cardioband Mitral System CE-mark trial recently presented 2-year data that showed 79% survival while MR $\leq$2+ for 96% of the patients. For technical success-rate, it is crucial to select the proper patients for this treatment. A discouraging factor is the long and cumbersome procedure which will dissuade cardiologists from its widespread adoption and the review goes on to conclude Cardioband has a long way to go before being ready for prime time (18) (13).

Figure 3- Cardioband device deployed, the implant is a polyester sleeve with radiopaque markers spaced 8 mm apart. Reprinted with permission from (19).

The first experiences of a transcatheter valve replacement for the mitral valve were transcatheter valve-in-valve (TViV) and valve-in-ring (ViR) procedures; essentially placing a TAVR device inside failed mitral bioprostheses and annuloplasty rings. Favorable clinical results with bioprostheses gradually led to them being chosen over mechanical valve more often, and with that came a need for re-operative valve replacements due to xenograft degeneration which still continues to rise. Repeating cardiac surgery to replace failed bioprostheses poses as a clinical challenge as these patients are frequently elderly, frail, have ventricular dysfunction, and the procedure carries significant morbidity and mortality risk even though surgery is considered the standard of care (20).

Feasibility of mitral ViV implantation was demonstrated and following studies acknowledged satisfactory clinical and hemodynamic outcomes at short- and midterm follow-up. The transapical access method also seemed fitting for mitral TViV (21)(22). These cases were mostly carried out with the balloon-expandable SAPIEN XT valve (Edwards, CA) and in 2014, the Edwards SAPIEN XT valve got CE Mark approval for transcatheter mitral ViV procedures (1). Deployment of a 26-mm Edwards SAPIEN XT valve (Edwards Lifesciences) into a degenerated 27-mm Carpentier-Edwards prosthesis in mitral position is shown in Figure 4. First in-man implantation of a TAVR in a mitral

annuloplasty ring was carried out shortly after the first ViV, however, studies show ViR poses unique and serious procedural challenges, specifically left ventricular outflow tract (LVOT) obstruction and post-procedural MR, and therefore has been linked to having more unfavorable outcomes in comparison with ViV (23).

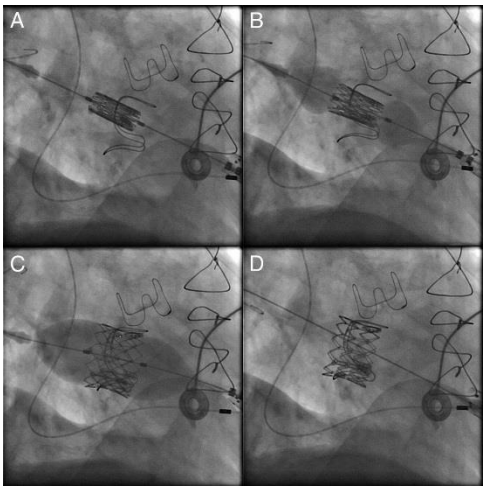

Figure 4-Positioning (A) and deployment (B to D) of a 26-mm Edwards SAPIEN XT valve (Edwards Lifesciences) into a degenerated 27-mm Carpentier-Edwards prosthesis in mitral position. Reprinted with permission from (21).

This limited experience shows a glimpse of the promise that transcatheter MV replacement (TMVR) can have in becoming the substitute for surgery in high risk MR patients, and its capacity to evolve into an easy and fast procedure that is applicable across the wide variations of patients and etiologies. However, there are many hurdles that should be overcome to design a device that successfully replaces the heart's most complex valve (1). These challenges and requirements are addressed in detail in Table 1.

Table 1- Complexity and challenges of developing a TMVR device

Challenges/Requirements for TMVR device development (1)	
Valve Anatomy	Asymmetrical saddle-shaped mitral annulus (compared to the circular aortic annulus)
	Lack of stable calcified structure for anchoring (unlike for TAVR)

	Complex subvalvular apparatus consisting of leaflets, annulus, chordae tendineae, and papillary muscles. Preservation of this structure is essential to maintaining LV geometry
	Irregular geometry of the mitral valve leaflets
Disease Heterogeneity	MR has multiple causes with different stages of severity and a variety of geometrical distortions in the LV anatomy as it progresses. Therefore, it is difficult to design a "universal device concept" tailored to target all potential MR types and patient profiles
Dynamic Environment	Dynamic changes throughout cardiac cycle in mitral annular geometry (shape/size) resulting in an overall reduction of annular area up to 30% and a reduction of annular circumference of up to 15%
	Maintaining device position within annulus, despite continuous cyclic movements and high transvalvular gradients (high dislodgment forces)
	Radial stiffness is needed in device to be stable the dynamic environment and avoid frame fracture, while keeping surrounding anatomy intact
Valve Location	Deployment in left AV is challenging due to a need for transseptal access and the need for a multidimensional, highly curved catheter course in order to get inside the left atrium
	The device should not obstruct the LVOT, occlude the circumflex coronary artery, compress the coronary sinus, or cause major conduction system disruption
Hemodynamic performance	Paravalvular leak (PVL) minimization is essential but valve sealing is a challenge due to the dynamic morphology of the mitral annulus, along with the high-pressure gradient generated by the ventricle during systole

The landscape of TMVR devices is currently quickly growing with over 30 devices under development, Table 2 lists a few of these devices. As seen in Table 2, there are significant differences amongst the devices in terms of valve design, position and anchoring mechanism. Images of each of these valves and their deployed state visualized under fluoroscopy are presented in Figure 6. A major concern for the replacement TMV is

making sure that it does not obstruct the LVOT. Reduction of LVOT area has been reported after surgical mitral valve procedures with prostheses and annuloplasty rings. Moreover, this has been witnessed even after transcatheter mitral interventions done with different devices. LVOT obstruction rate secondary to transcatheter mitral ViR is reported as 8.2%, rising to 9.3% if the mitral annulus is severely calcified (24). This risk intensifies with intra-annular designs that venture into the LV space and requires careful observation and comparison with the supra-annular models. Figure 5 displays the different anatomical and device design issues that can lead to LVOT obstruction.

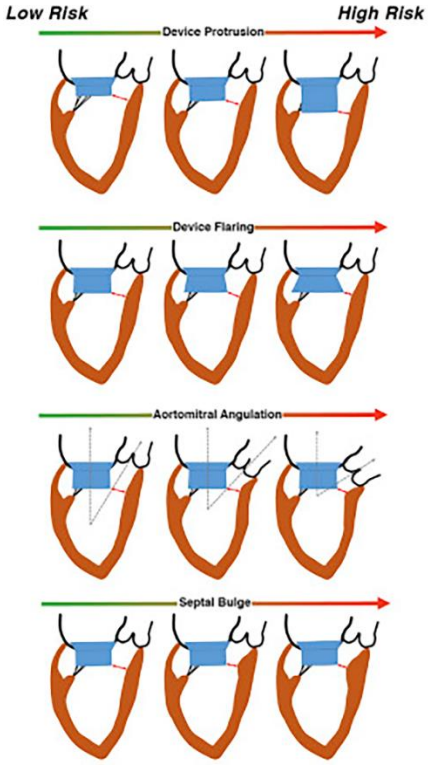

Figure 5-Greater device protrusion into the left ventricle, device flaring at its left ventricular outflow, larger aorto-mitral angulation, and more pronounced septal bulging can lead to LVOT obstruction. Reprinted with permission from (25).

For the purpose of this discussion, two of the devices that are furthest along in clinical evaluation and the design that is modeled in this work are discussed below.

Tendyne™ Mitral Valve System: The Tendyne™ device (Tendyne™ Mitral Valve System, Abbott Structural, Santa Clara, CA) is an intra-annular, D-shaped, tri-leaflet, self-expanding porcine pericardium valve placed within a nitinol prosthesis with transapical transcatheter delivery and is fully retrievable. The device uses a polyethylene tether for anchoring to the LV apex and has an asymmetric, D-shape sealing cuff. In the early feasibility trial, 100 patients with grade 3 or 4 MR and mostly secondary (89%) received the Tendyne system. Risk of open surgery was prohibitive for all patients. In 96 patients, the device was deployed successfully, and no mid-procedure were reported. At 30 days, 6 deaths (6%) and 2 strokes (2%) happened. The all-cause mortality and cardiac mortality were 27.6 % and 15.4% respectively at 1-year. At 1-month in 98.8% of patients the MR degree was none or trivial, and at 12-months in 98.4%. The US pivotal trial of this device has been initiated based on these results and in early 2020 received CE Mark and got approved for use in Europe (25)(13)(26). Figure 6, U and W show this device.

Intrepid™ TMVR System: The Medtronic Intrepid™ valve system (Intrepid™ TMVR System, Medtronic, Inc., Redwood City, CA) is an intra-annular, circular, tri-leaflet, self-expanding bovine pericardium valve placed on a nitinol stent with transapical transcatheter delivery. Radial forces and a barbed metal frame are used for anchoring the device within the mitral annulus. In the early experience with this device, 50 patients with symptomatic, severe MR received the device with successful implantation in 96% of patients. Figure 6, M and N show this device. The 30-day mortality was 14% with no disabling strokes or repeat interventions and at a follow-up of 173 days, only mild or no residual MR was reported. The US pivotal trial APOLLO has been formed following these results. This trial is an ongoing study that has two parts, the first part randomizes severe,

symptomatic MR patients who have acceptable surgical risk to TMVR vs. conventional surgery (n=650) and in the second, patients with prohibitive surgical risk get TMVR (n=550) (25)(13)(26).

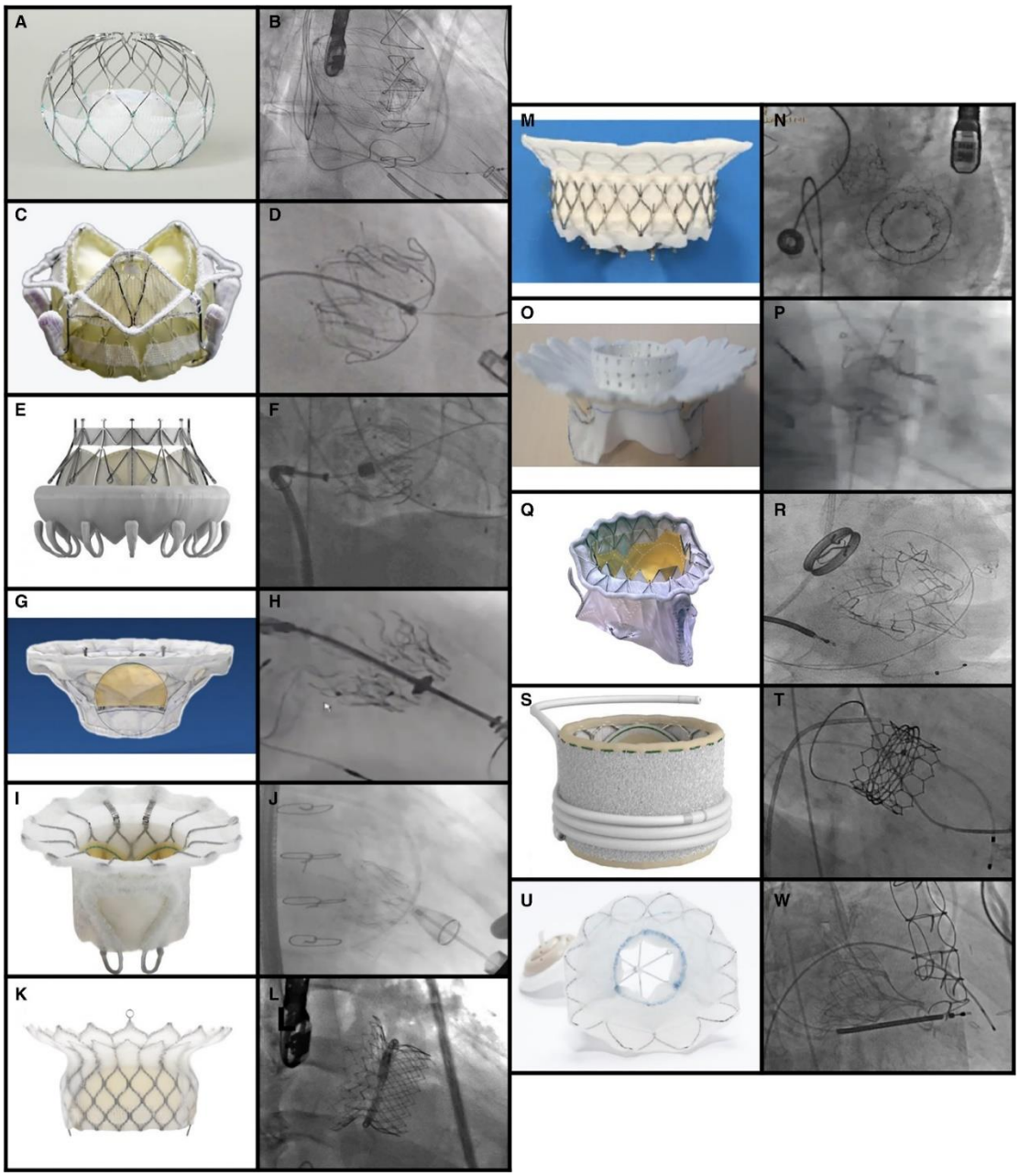

Figure 6- Transcatheter mitral valve replacement (TMVR) devices. ***A,*** *AltaValve.* ***B,*** *Fluoroscopic image of the AltaValve.* ***C****, Caisson TMVR.* ***D,*** *Fluoroscopy image of the Caisson TMVR.* ***E,***

CardiAQ Valve. ***F,*** *Fluoroscopy image of the CardiAQ Valve.* ***G,*** *CardioValve.* ***H,*** *Fluoroscopy image of the CardioValve.* ***I,*** *Fortis.* ***J,*** *Fluoroscopy image of the Fortis.* ***K,*** *HighLife.* ***L,*** *Fluoroscopy image of the HighLife.* ***M,*** *Intrepid TMVR.* ***N,*** *Fluoroscopy image of the Intrepid TMVR.* ***O,*** *MValve System.* ***P,*** *Fluoroscopy image of the MValve System,* ***Q,*** *Neovasc Tiara.* ***R,*** *Fluoroscopy image of the Tiara.* ***S,*** *Sapien M3 System.* ***T,*** *Fluoroscopy image of the Sapien M3 System.* ***U,*** *Tendyne.* ***W,*** *Fluoroscopy image of the Tendyne. Reprinted with permission from* (27).

Table 2-Overview of TMVR designs under clinical testing and development

Device	Design	Valve Position	Access	Anchoring Mechanism
Tendyne	D-shaped (Outer stent) Circular (Inner frame)	Intra-annular	Transapical	Apical Tether
Intrepid	Circular	Intra-annular	Transapical	Radial forces and sub-annular cleats
Neovasc Tiara	D-shaped	Intra-annular	Transapical	Native leaflet engagement, ventricular anchors to grasp the free margins of the native leaflets
Sapien M3	Circular	Intra-annular	Transseptal	Modified Sapien 3 with dock
CardiAQ-Edwards	Circular	Polyester fabric(Supra-annular), Sealing skirt (Intra-annular)	Transapical transseptal	Mitral annular clamping with atrial and ventricular flanges acting as opposing anchors
Caisson	D shape	Supra-annular	Transseptal	External anchor mitral annulus capture, with engagement at sub-annular fibrous groove

HighLife TMVR	Circular	Sub-annular ring implant	Transapical (Femoral artery for guidewire)	External anchor mitral annulus capture
AltaValve System	Circular	Supra-annular with fabric skirt to prevent perivalvular leak	Transapical	Nitinol frame of spherical shape
Fortis	Circular	Intra-annular	Transapical	2 Opposing paddles

Sapien M3™: The Sapien M3™ valve system (Sapien M3, Edwards Lifesciences, Irvine, CA) is an intra-annular, circular, bovine pericardium valve that is balloon-expandable, placed on a cobalt-chromium frame that is fixed in position with a nitinol coiling system wrapped around the native mitral valve leaflets and uses a transseptal transcatheter delivery. This design is based on the successful Sapien 3 TAVR prosthesis, with an added polyethylene terephthalate skirt to ensure a seal is formed between the nitinol docking system and the native valve. 10 patients with severe primary, secondary or mixed MR were considered for the initial in-human study. 9 cases had successful implants, and trivial or no MR was reported in all cases. 30-day outcomes showed no unfavorable cases of rehospitalization, stroke, left ventricular outflow tract obstruction, myocardial infarction, embolization, device migration or conversion to open surgery although a paravalvular leak was developed in one case, which was then treated with a closure device. This was a demonstration of Sapien M3 valve feasibility and safety for high surgical risk patients with severe MR (25). Figure 6, S and T show this device.

Although by now the necessity and feasibility of a TMVR has been proven, it is essential to understand the modes of failure and the durability of the device in order to

consider it as a standard of care. The intention of any medical treatment is to provide the patient with the optimal long-term cure or relief. Therefore, heart valve prosthesis long-term durability should preferably be longer than the expected lifespan of the patient it is being used for (28). The International Organization for Standardization currently requires valve prostheses to meet certain durability targets before certifying them for commercialization. Each valve must undergo a certain amount of sterilization cycles, at least 200 million cycles (equaling 5 years of durability)(29). Undoubtedly, with the limited clinical experience of TMVR devices, the actual durability and failure modes are still not identified and there is great need for research and knowledge in this area. Even for TAVR devices, this information is not adequate as this treatment has only become prevalent since obtaining FDA approval in 2011 and not even a ten year durability analysis is possible (29).

Some insight can be drawn from surgical aortic valve replacements and studies that have been done with TAVR for a 5-year outcome. In general, bioprosthetic surgical aortic valves have had a more favorable hemodynamic performance in comparison with mechanical aortic valves and have the advantage of not needing life-long anticoagulation therapy, but fall short in terms of durability as a result of calcification and/or fatigue-related structural degeneration (30). Both surgical and transcatheter bioprostheses are made from biological tissues such as bovine or porcine pericardium and are at a risk of structural valve degeneration (SVD), a multifactorial process that results in the calcification and degeneration of the leaflets which ultimately lead to valve stenosis, leaflet tear and regurgitation (29). The most common failure mechanisms that have been witnessed among the reported cases of transcatheter heart valve (THV) SVD are tissue ingrowth (pannus),

incomplete THV expansion and leaflet calcification (31). Increased leaflet mechanical stress has been identified as one of the main mechanisms in the pathogenesis of SVD that cause the valve leaflet tissues to be thickened (29). Moreover, in a finite element analysis of leaflet fatigue due to cyclic loading that compared a transcatheter aortic valve (TAV) and a surgical aortic valve (SAV) with same loading conditions. In comparison with the SAV leaflets, higher stresses, strains, and fatigue damage was witnessed in the TAV leaflets (30). Therefore, it is essential to identify and understand any condition that can induce higher mechanical stress on transcatheter valve leaflets as it may accelerate SVD. The first aim of this work is to quantify the stress distribution on a potential TMVR design and compare to a surgical mitral valve replacement device under the same loading conditions.

Valve thrombosis is another common mechanism of failure that occurs in bioprosthetic valves (32). In patients undergoing surgical aortic valve replacement (SAVR), thrombosis can happen in the early postprocedural phase in up to 15% of cases. Several theoretical mechanisms have been proposed to explain why risk of thrombosis in THVs could potentially be higher than SAVR: 1) comorbid prothrombotic conditions such as cancer, 2) the metal THV frame is a potential cause of thrombosis, 3) under-expansion of the valve can cause folds in the leaflet resulting in potential spots for thrombosis, 4) native leaflets may create regions of reduced blood flow and stagnation (31). Although thrombosis is usually treated successfully with anticoagulant therapy, it can also lead to inflammation and consequent calcification of the leaflets (29) and studies have expressed that currently, the optimal management of THV thrombosis is still not clear (31).

Therefore, it is crucial to study and understand the risk of thrombosis and its causes in THVs.

Currently, blood residence time (BRT) and wall shear stress are recognized as factors related to thrombus formation, providing a method of quantifying risk of thrombosis in computational simulations. High wall shear stress (WSS) results in platelet activation, hemolysis, and endothelial cell damage and is related to thrombotic risk. Conversely, regions of flow recirculation are linked to lower WSS and high residence time (RT), and combined with prior high shear stress exposures, might potentially add to thrombus formation risk. WSS, a measure of red blood cell exposure to different shear conditions, has previously been reported as an important factor for comparing various anatomies and clinical scenarios. In this context, RT is a way of quantifying fluid stagnation in a specific location, helping to give a time frame in the process of thrombus formation (33). The next aim of this work is to quantify BRT and understand the risk of thrombosis in TMVR devices. As explained previously, TMVR designs can be in either supra-annular or intra-annular position, and this study aims to compare the risk of thrombosis between these two designs and ultimately compare the risk of thrombosis to that of a surgical mitral valve replacement device. For that purpose, a computational model of the left atrium and ventricle will be built that incorporates the movement of the left ventricle and the valve leaflets during the cardiac cycle in order to fully resemble the flow field within the valve and left ventricle.

CHAPTER TWO: MATERIALS AND METHODS

TMV performance is assessed through understanding leaflet stress distribution and making precise flow measurements close to the TMV leaflets, which pose challenges in the clinical settings as the imaging modalities that are currently available are limited in temporal and spatial resolution. Therefore, to investigate the stress distribution and flow field around the TMV device in intra and supra-annular positions, a combination of computational modelling and experimental testing were utilized. The method is explained step by step.

2.1. Geometry

The first step to building the computational models was designing the valve and LV geometry. For the surgical mitral valve replacement, a 25-mm Carpentier-Edwards (CE) PERIMOUNT Magna mitral valve (Edwards Lifesciences, CA) device was used. This surgical bioprosthetic valve has a 24 mm Elgiloy frame that the bovine pericardium leaflets are mounted on. As no TMV is commercially available, for the TMV models, the 26-mm Edwards SAPIEN 3 (Edwards Lifesciences, Irvine, CA) device was used to construct the SAPIEN M3 (Edwards Lifesciences, Irvine, CA) TMV design. The SAPIEN M3 valve has a balloon-expandable cobalt-chromium stent exactly like the SAPIEN 3 with bovine pericardial leaflets mounted on the stent.

The SAPIEN M3 also has a polyethylene terephthalate skirt around it ensuring a seal is made between the docking system and the valve, therefore that was also built around the valve. Both valves can be seen in Figure 7. A Mitutoyo Digital caliper (Mitutoyo Corp, Kanogawa, Japan) was used to measure the leaflet thickness; average thicknesses of 0.50, and 0.32 mm were reported for CE PERIMOUNT Magna bioprosthesis, and SAPIEN 3, respectively.

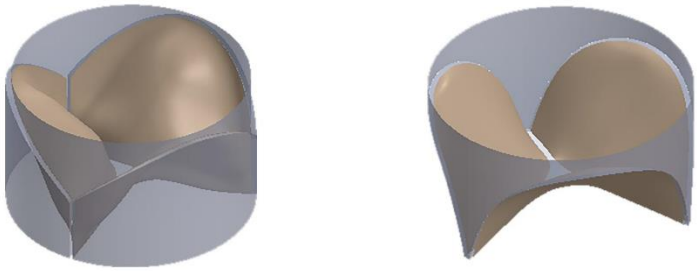

Figure 7- Geometry of a) Edwards SAPIEN 3 and b) CE PERIMOUNT Magna valves built with Solidworks. The grey area identifies the stent around the leaflets shown in beige

Patient-specific anatomical CT data of the left side of the heart were obtained over one full cycle from a patient in heart failure with an ejection fraction of 0.35. Image segmentation was done with Mimics Materialise software to build a 3D model as seen in Figure 8a. Initial surface smoothing was done with Mimics to generate the initial mesh file output as seen in Figure 8b. The mesh was then exported to Geomagic Design to fit a surface to the smoothed mesh, Figure 8c. Finally, after obtaining a full smoothed surface of the model, the aortic root and aorta were cut from the model as they were irrelevant to the TMV simulation and to simplify the analysis, Figure 8d. The four pulmonary veins entering the left atrium are the inlets of the model and the aortic root is the outlet. The valves were then placed inside the left heart model. Three models were built with

Solidworks: 1) THV in intra-annular position, 2) THV in supra-annular position and 3) a surgical mitral valve in intra-annular position. All three models are seen in Figure 9.

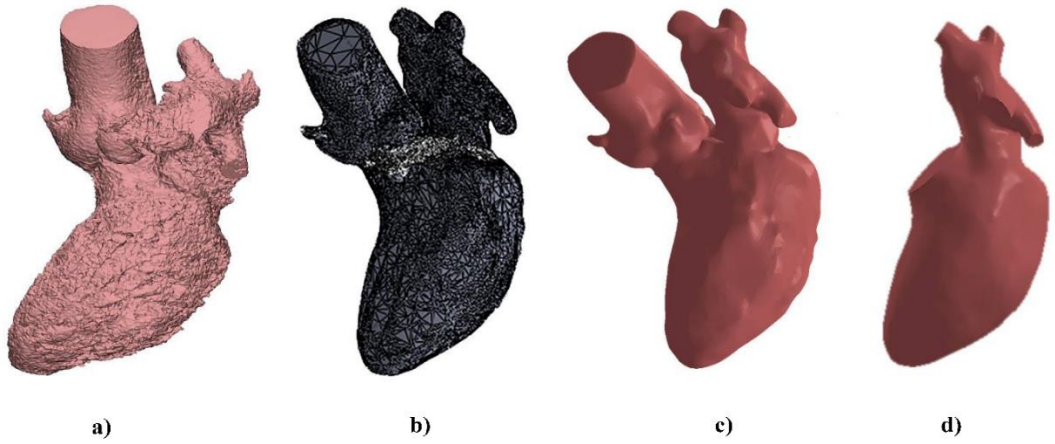

Figure 8- Stages of building left heart computational model: a) rough model obtained after segmentation, b) smoothed mesh output from Mimics, c) surface fitted to the mesh with Geomagic Design and d) final left heart model after removing aorta at the aortic root

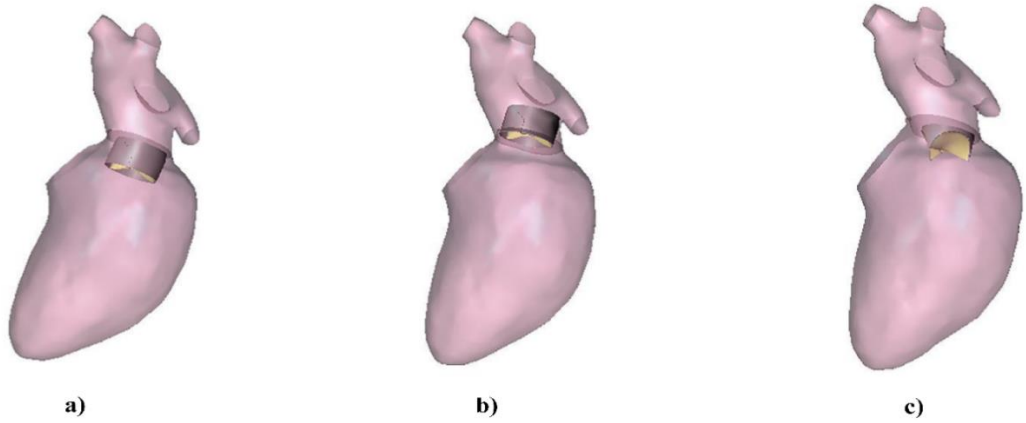

Figure 9- Final computational models with transcatheter valve (Edwards SAPIEN 3) placed in a) intra-annular position, b) supra-annular position and surgical valve (CE Perimount Magna) placed in intra-annular position

2.2. Experimental Setup

2.2.1. *In Vitro Pulse Duplicator System*

For the computational simulations, the pressure gradient on the mitral valve device was necessary for each of the two valves with physiological loading conditions. Each

bioprosthetic heart valve was placed in the pulse duplicator system (BDC Labs, Wheat Ridge, CO) in mitral position. The Carpentier-Edwards PERIMOUNT Magna mitral bioprosthesis is positioned on a silicone washer and the sewing ring is sutured to it to hold the valve in position. In addition, the SAPIEN 3 TAV was put inside a silicone washer, making sure that the TAV frame (stent) bottom was level with the silicone washer bottom. In the aortic valve position, a bileaflet mechanical heart valve is put in the silicone ventricle to maintain aortic outflow. A picture of the setup is provided below in Figure 10. The input parameters for the pulse duplicator were in accordance with the international standard ISO 5840: 2015 recommendations for testing prosthetic heart valves; that is, heart rate of 70 beats/min, mean aortic pressure of 100 mm Hg, and cardiac output of 5 L/min. The peripheral resistance in the setup and the compliance are controlled to ensure physiological flow conditions. When the pump's piston moves during every stroke, the pressure around the compliant silicone ventricle changes, ejecting the flow through the aortic valve. As a blood analog fluid, a recirculating fluid of 45% by volume glycerin solution (99% The Science Company, Denver, CO, USA) in phosphate buffered normal saline solution (Research Products International, Mount Prospect, IL, USA) was used. The running solution has a viscosity of 3.45 cP, a density of 1.12 g/cm^3, and a refractive index of 1.39 at 37°C. To measure the pressure in the atrium and left ventricle, strain gauge pressure transducers (Utah Medical Products, Midvale, UT, USA) were positioned inside the pulse duplicator at 35 mm downstream and 105 mm upstream of the bioprostheses in mitral position. Prior to the tests, the pressure transducers were calibrated with Delta-Cal Pressure transducer simulator/tester (Utah Medical Products, Inc). In addition, an electromagnetic flowmeter (Model 501,Carolina Medical Electronics Inc, East Bend, NC, USA) was used

to measure flow rate in the system. Specific details on the in-vitro testing were obtained from (34).

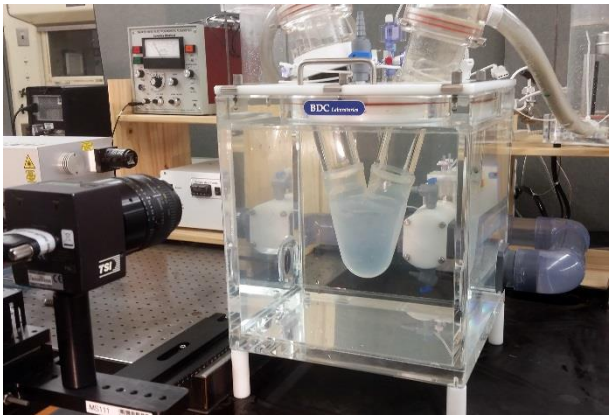

Figure 10-Pulse duplicator experimental setup, the silicon heart chamber can be seen.

During the experiment, leaflet motion is captured with a high-speed camera (Sony DSC-RX10M3) positioned underneath the mitral valve position at a rate of 960 frames per second. The images were digitized in Solidworks; for each leaflet edge, the center point was tracked during the full cardiac cycle, calculating the distance of the tip from the center of the valve. The values from all three leaflets were averaged and used as the displacement curve of the leaflet. Sample images obtained during the experiment can be seen in Figure 11.

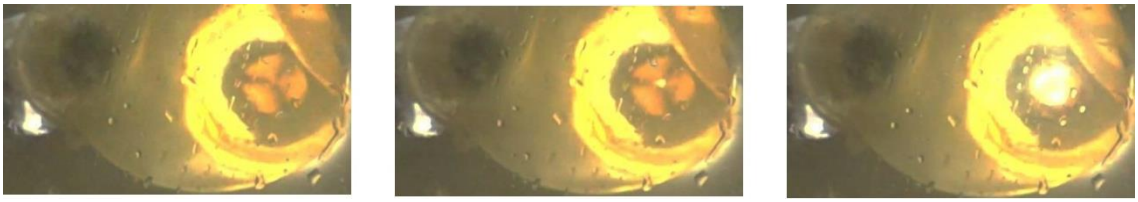

Figure 11-Photos obtained of the valve motion during the experiment

2.3. Computational Simulations

2.3.1. Finite Element Modeling: Leaflets

The leaflet geometry for the bioprosthetic valves was found through 3D scanning of the geometry, a NextEngine 3D Laser Scanner (resolution of 100 micrometers, NextEngine, Inc., Santa Monica, CA) was used. RapidWorks and SOLIDWORKS packages were used for the surface reconstruction of valves. One leaflet geometry was reconstructed, and mirrored using symmetry for the other two leaflets. The leaflets' IGES formats were obtained for FE simulation. Subsequently, the leaflets underwent mesh generation with HyperMesh (Altair Engineering, Inc., Troy, MI), in which a mapped mesh was used to discretize the geometry. After that, the mesh was taken into ABAQUS/Explicit solver. The geometry of CE PERIMOUNT Magna and SAPIEN 3 leaflets were meshed using 6924 and 6714 ABAQUS S4 shell elements, respectively. The element size in the simulations was determined based on displaying mesh density independence, with less than 1% difference. The mesh for each of the leaflets is presented in Figure 12.

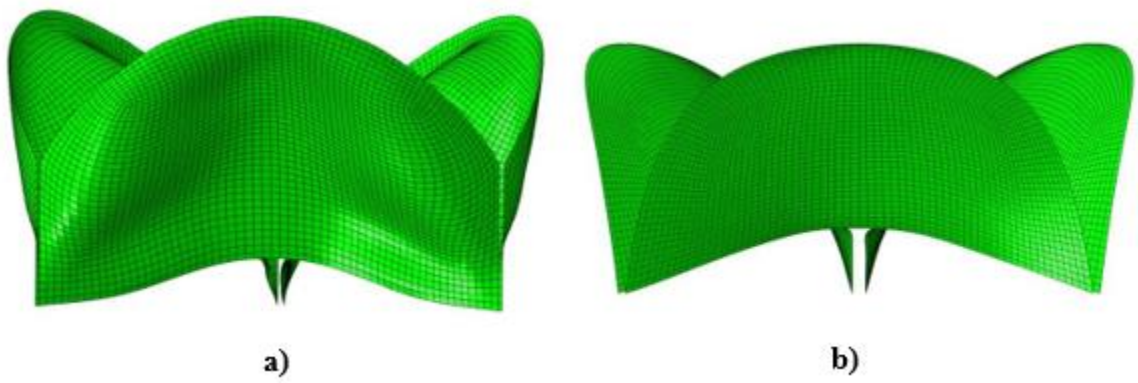

Figure 12-Mesh of valve leaflets, a) SAPIEN 3 and b) Perimount Magna

It was assumed that throughout the leaflet, leaflet thickness is uniform and constant, equivalent to 0.50, and 0.32 mm for CE PERIMOUNT Magna bioprosthesis, and SAPIEN 3, respectively. A MATLAB code was written to find the material orientation of the shell elements. The leaflet density was 1100 kg/m^3. On the atrial side of the leaflets, the pressure

gradient waveforms obtained across the valve from the experimental tests were applied. In addition, to resemble viscous damping effects of surrounding fluid, a Rayleigh damping coefficient α was added. In the ABAQUS/Explicit package, a form of strain energy potential provided to characterize anisotropic materials is the generalized three-dimensional Fung strain-energy function. The bioprosthetic leaflets were assumed to be pseudo-hyperelastic anisotropic materials in the FE simulations.

The general Fung strain-energy function is:

$$\Psi = \frac{c}{2}(e^{Q} - 1) + \frac{1}{D}\left(\frac{J_{el}^2 - 1}{2} - \ln J_{el}\right)$$

where Ψ is the strain energy per unit of reference volume. D and c describe the temperature-dependent material parameters, J_{el} stands for the elastic volume ratio and Q is given by:

$$Q = E : (\mathbb{b}E)$$

where $\mathbb{b}$ is a non-dimensional symmetric fourth-order tensor with 21 independent components, and E is the Green–Lagrange strain tensor.

$$\mathbb{b}_{anisotropic} = \begin{bmatrix} b_{1111} & b_{1122} & b_{1133} & b_{1123} & b_{1113} & b_{1112} \\ & b_{2222} & b_{2233} & b_{2223} & b_{2213} & b_{2212} \\ & & b_{3333} & b_{3323} & b_{3313} & b_{3312} \\ & & & b_{2323} & b_{1323} & b_{1223} \\ & & & & b_{1313} & b_{1213} \\ & & & & & b_{1212} \end{bmatrix}$$

As the material is assumed to be incompressible, (J_{el} = 1), the Fung strain energy function changes to:

$$\Psi = \frac{c}{2}(e^{Q} - 1)$$

2.3.2. Optimization Framework: Leaflets

A global optimization approach was implemented to obtain the 3D mechanical properties of the leaflets. Initial estimate values for optimizing Fung's model were taken from Abbasi et al (34). Executed in Isight (Simulia, Providence, RI), a particle swarm optimization (PSO) method (34) is used to identify the optimized leaflet material parameters as well as the viscous damping coefficient. The hemodynamic data from experiments with the pulse duplicator setup was used for the optimization. The displacement of the midpoint on the leaflet edge from the experiments in the pulse duplicator system was used as a target to match the displacement of the same point in the FE simulation. The objective function is defined as the sum average of the squared differences between the displacement values of the simulation results and experimental results. To increase computational efficiency, only one leaflet motion during one cardiac cycle was simulated. The optimization process ended once the objective function value dropped below 5×10^{-5}. For optimizing the material properties of each valve leaflet, the pressure obtained from experiments with the respective valve was used.

2.3.3. Finite Element Simulation: Leaflets

After finding the optimized material property parameters, the leaflet simulation was run under physiological loading conditions. For a fair comparison of stress values between the two valves' leaflets, physiological loading conditions consisting of simultaneously acquired LA and LV pressures throughout one cardiac cycle was obtained from (35), enabling the calculation of the pressure gradient across the mitral valve. It should be noted

that these pressures were obtained from patients undergoing first-time coronary bypass surgery and had either trivial or mild mitral regurgitation. The mean ejection fraction among the patients was 0.38±0.19. A Savitzky-Golay smoothing filter with an order of five was applied to the data to get rid of unwanted noise.

2.3.4. Finite Element Modeling: Left Ventricle (LV)

In order to simulate the LV motion during the cardiac cycle, a finite element model of the LV was built. The geometry was meshed with S3 elements with a mesh size of 1 mm and a total of 62381 elements. The majority of patients undergoing TMVR in clinical trials have a left ventricular ejection fraction (LVEF) of between 30-40% (24). The patient in question had an approximate ejection fraction of 35%. Geometric models were built for each time frame that the CT scans provided and were used as a guide for LV contraction and expansion simulation. The end-diastolic state, when the heart is at its largest and is full of blood ready to be pumped, was considered as reference, and displacement in respect to this reference point was considered. An image of the LV at end diastolic and end systolic position are provided in Figure 13.

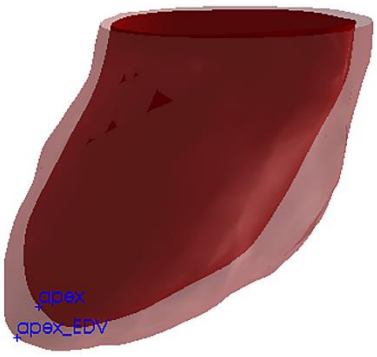

Figure 13-LV in fully expanded and contracted configuration with an ejection fraction of 0.35. The apex at end systolic volume (apex) and end diastolic volume (apex_EDV) can be seen

The material was assumed to be hyperelastic and a reduced polynomial strain energy function was used. The form of the reduced polynomial strain energy potential (N=4) is:

$$\Psi = \sum_{i=1}^{4} C_{i0}(\bar{I}_1 - 3)^i + \sum_{i=1}^{4} \frac{1}{D_i}(J_{el} - 1)^{2i}$$

where Ψ is the strain energy per unit of reference volume. D_i and C_{i0} stand for the temperature-dependent material parameters, J_{el} describes the elastic volume ratio, and $\bar{I}_1$ is the first deviatoric strain invariant. To simulate viscous damping effects of the surrounding fluid, a Rayleigh damping coefficient α is added to the model. Compressibility can be defined by specifying nonzero values for D_i . Initial guesses for the model were derived from the experimental stress/strain data found in (36) through fitting the hyperelastic material model in ABAQUS.

2.3.5. Optimization Framework: LV

In order to simulate LV contraction, the position of the apex was tracked during the cardiac cycle and use as the target for optimization. A global optimization framework was used to match the apex displacement of the computational model to the observation from the CT derived models. The apex at the two states can be seen in Figure 13. The LV material parameters were optimized with a particle swarm optimization (PSO) algorithm (34) executed in Isight (Simulia, Providence, RI). The apex displacement in x, y, z in the FE simulation was optimized with the results of the apex displacement in x, y, z during the cardiac cycle. The objective function in the optimization procedure minimizes the average

of the sum of the squared differences for the displacement from CT data and simulation results. Once the objective function drops below 5×10^{-5}, the optimization process ends.

2.3.6. Finite Element Simulation: LV

After finding the optimized material property parameters, the leaflet simulation was run under physiological loading conditions for the LV obtained from (35). It should be noted that the purpose of this simulation is solely to simulate the LV movement and values of stress are irrelevant, only displacement values are of interest.

2.3.7. Computational Fluid Dynamics (CFD) Modeling

The aim of CFD modeling is to use one-way Fluid-Structure Interaction (FSI) simulations to simulate the three-dimensional flow field of the TMVs in ANSYS Fluent (ANSYS, Canonsburg, PA, USA). The fluid domains were discretized into unstructured tetrahedral elements using Pointwise (Pointwise Inc., Fort Worth, TX, USA). The number of elements in the simulations were determined based on displaying mesh density independence, with a difference of less than 1%. Blood was considered a Newtonian fluid with density and the viscosity of 1,060.0 kg/m^3 and 0.0035 $kg.s/m^2$, respectively. Initially, steady-state simulations of the surgical, intra-annular and supra-annular models were run to get a preliminary visualization of the flow field. A constant inlet pressure of 1600 kPa, equivalent to the inlet pressure of the left atrium was used. The pressure at outlet was assumed to be zero. A k-epsilon turbulence model was used to simulate the turbulent flow. The residuals were monitored to reach 1×10-6. However, the movement of the leaflets and LV need to be incorporated into the CFD model in order to fully simulate the left heart during the cardiac cycle. Codes were written to create frames of the leaflet movement from the FE simulation of the leaflets. For each leaflet, a fine cloud mesh is generated at every

0.2 ms based on the FE simulation. The same was done for the LV. Consequently, a user-defined function (UDF) uses the cloud meshes to update the leaflets' surface grids at each time-step. ANSYS Fluent has a dynamic mesh feature that includes a cell size/skewness-based remeshing scheme and a diffusion-based smoothing, both of which are used at each time-step to update the mesh of 3D tetrahedrons in the computational grid. Tecplot 360 (Tecplot USA, Bellevue, WA, USA) was used to visualize the results

CHAPTER THREE: RESULTS

3.1. Experimental Results

After testing the two bioprosthetic heart valves with the pulse duplicator, the results of the flow and pressure waveforms are shown in Figure 14. The effective orifice area of the bioprostheses was calculated based on the Gorlin equation. The bioprosthesis effective orifice area is 2.03 ± 0.029cm^2 for Edwards SAPIEN 3 and 1.75 ± 0.024 cm^2 for CE Perimount Magna.

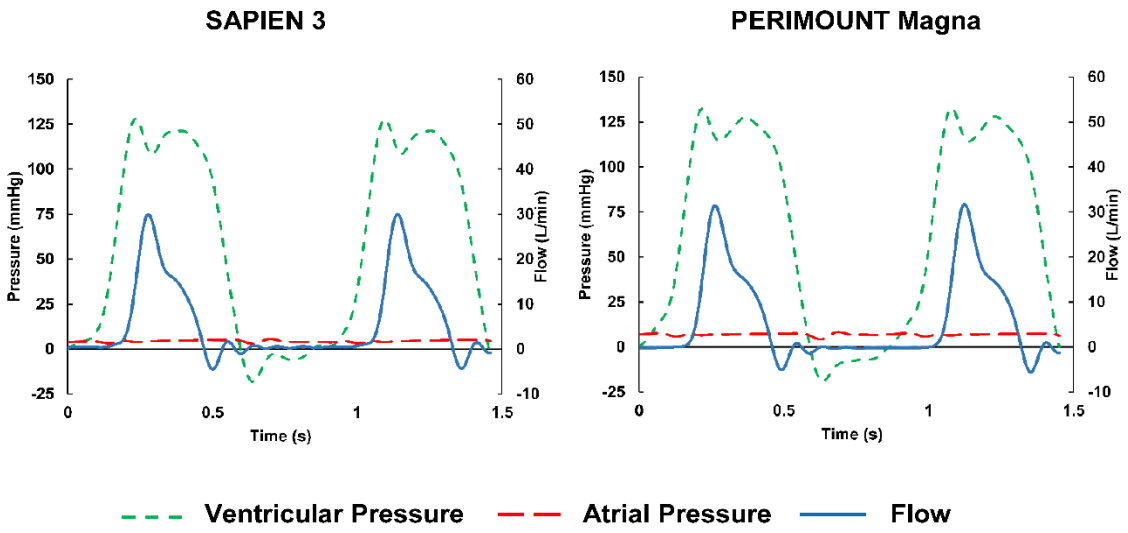

Figure 14-Raw pressure and flow waveforms obtained from experimental testing of each valve with the pulse duplicator test setup

The pressure waves were used to find 3D mechanical properties in the optimization procedure for the two valve leaflets. Initial estimates were taken from a study (34) for the valves in aortic position. Using PSO method in Isight, the displacement of the midpoint on the leaflet edge in the FE simulation was matched to the averaged experimental data through optimizing the Fung model parameters of the leaflets and the Rayleigh damping coefficient. In the optimization procedure, just one leaflet motion was fitted to the averaged displacement curve. The sum of the squared difference of the simulated and measured displacement for the midpoint of the leaflets was minimized through changing material parameters. The optimized 3D anisotropic Fung model material parameters are shown below in matrix format. Furthermore, the estimated values for the material parameter, c and viscous damping, α in the Fung model are presented in Table 3. Optimization results are seen in Figure 15. It took around 500 iterations for the optimization results to become in agreement with the experimental data. In addition, in Figure 15, the results of using the initial material properties from (34) are plotted with the results obtained from the optimized material parameters.

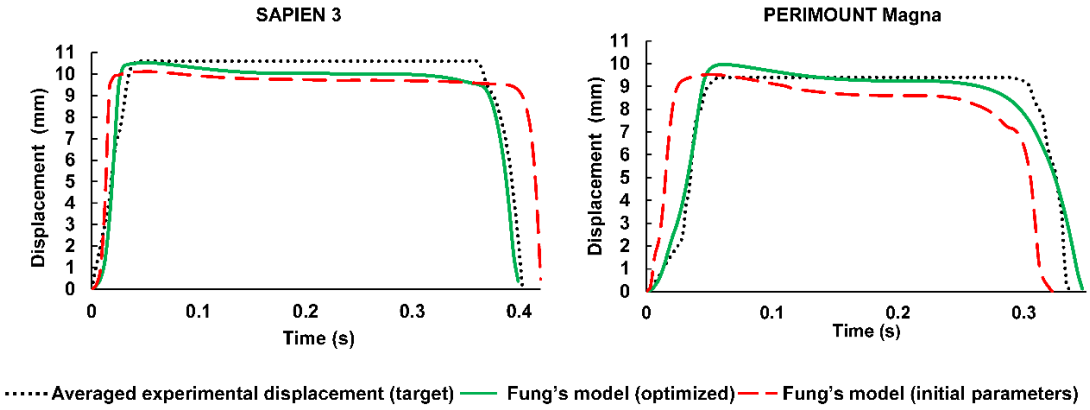

Figure 15- Optimization results for the averaged leaflet tip displacement for each valve. Each graph compares the optimized FE simulations with the experimental data and simulation with initial parameters

Table 3-Material parameter and viscous damping coefficient for 3D anisotropic Fung model

Bioprosthesis	c (material parameter, Pa)	α (viscous damping, 1/s)
CE PERIMOUNT Magna	28338	14695
SAPIEN 3	24587	8278

$$\mathbb{b}_{Perimount\ Magna} = \begin{bmatrix} 62.25 & 33.50 & 53.90 & 16.50 & 51.50 & 41.40 \\ & 63.60 & 44.40 & 65.43 & 61.66 & 18.34 \\ & & 62.71 & 40.50 & 63.00 & 54.71 \\ & & & 13.90 & 15.71 & 29.50 \\ & & & & 44.90 & 13.79 \\ & & & & & 64.32 \end{bmatrix}$$

$$\mathbb{b}_{Sapien\ 3} = \begin{bmatrix} 80.52 & 37.37 & 61.00 & 20.31 & 40.00 & 38.91 \\ & 78.30 & 45.03 & 74.76 & 73.96 & 25.82 \\ & & 86.30 & 40.32 & 64.70 & 53.04 \\ & & & 14.49 & 15.14 & 26.62 \\ & & & & 46.08 & 17.44 \\ & & & & & 65.42 \end{bmatrix}$$

3.2. Finite Element Analysis Results

3.2.1. Leaflet Stress Distribution

The maximum in-plane principal stress distribution for 25-mm CE PERIMOUNT Magna and 26-mm SAPIEN 3 utilizing the optimized parameters were obtained with the same physiological loading on both valves for a fair assessment of stress values. Stress distribution is shown separately for SAPIEN 3 during systole and diastole in Figure 16 ,a, b and Figure 17 a, b, respectively and for CE PERIMOUNT Magna in Figure 16 c, d and Figure 17 c, d. To make sure stress values are independent of the cycle, two cardiac cycles were simulated. During systole, the boundary edges for the two valve leaflets had higher stress areas compared to the rest of the leaflet. The maximum stress value on the leaflet during systole reached to 4.75 and 16 MPa for the CE PERIMOUNT Magna, and SAPIEN 3, respectively. In diastole, the maximum stress recorded for the PERIMOUNT Magna and

SAPIEN 3 leaflets was 0.19 and 0.23 MPa, respectively. For both valves, regions of high stress were located around the commissures at the tip of the leaflets and in the mid-bottom section of the leaflets in the full open state. The maximum in-plane strain distribution of 26-mm SAPIEN 3 and 25-mm CE PERIMOUNT Magna are also shown in Figure 18 during systole and Figure 19 for diastole. At systole, the maximum leaflet strain value for the CE PERIMOUNT Magna, and SAPIEN 3 was 0.33 and 0.25, respectively. During diastole, the maximum strain value was 0.13 and 0.11, for PERIMOUNT Magna and SAPIEN 3 leaflets, respectively. With the PERIMOUNT Magna valve, high strains are seen in the mid-belly region of the leaflet, but maximum values during systole, like with stress, are seen closer to the commissures.

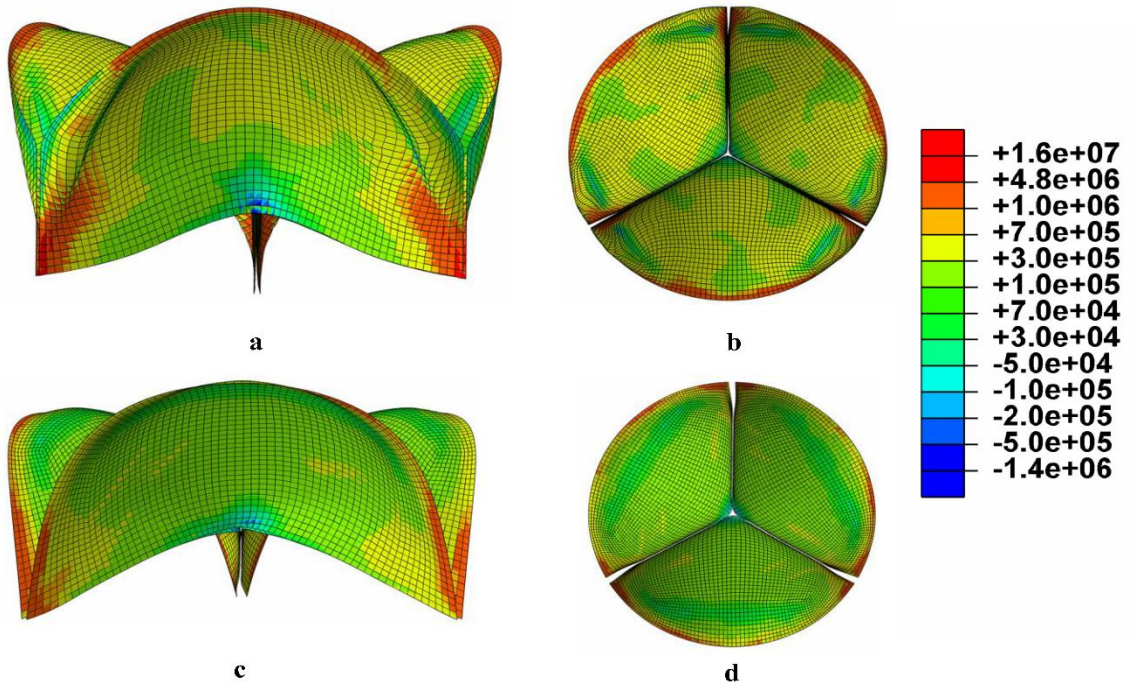

Figure 16- Maximum in-plane principal stress at peak systole, a) side view, b) bottom view SAPIEN 3, c) side view, d) bottom view PERIMOUNT Magna

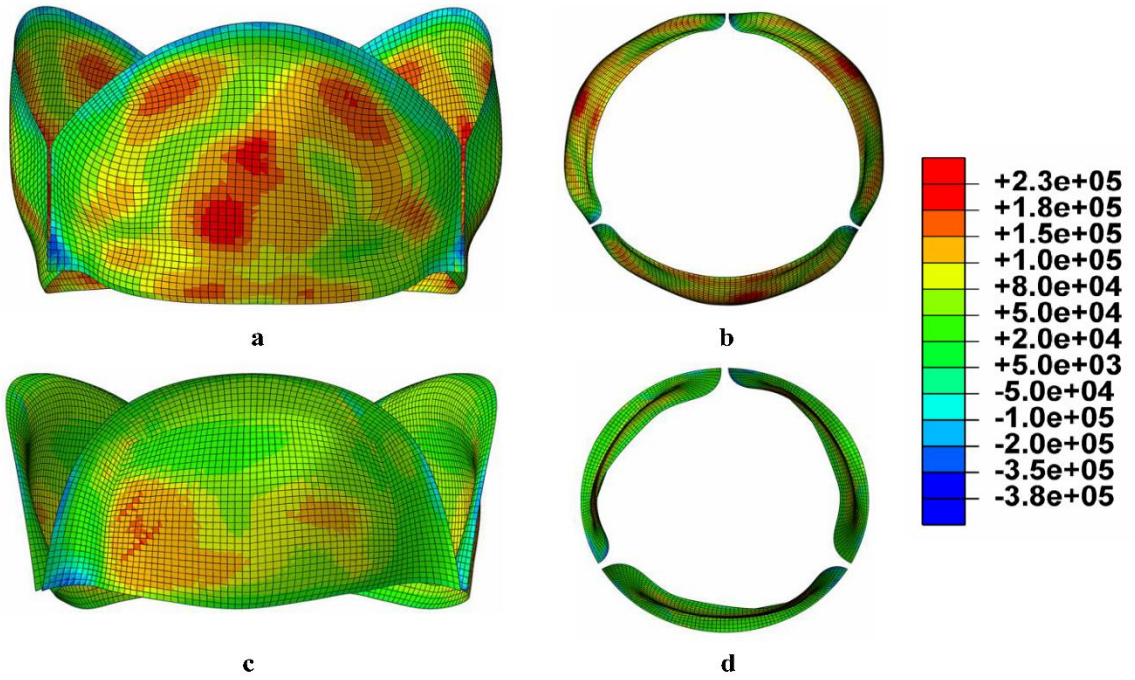

Figure 17-Maximum in-plane principal stress at peak diastole, a) side view, b) bottom view SAPIEN 3, c) side view, d) bottom view PERIMOUNT Magna

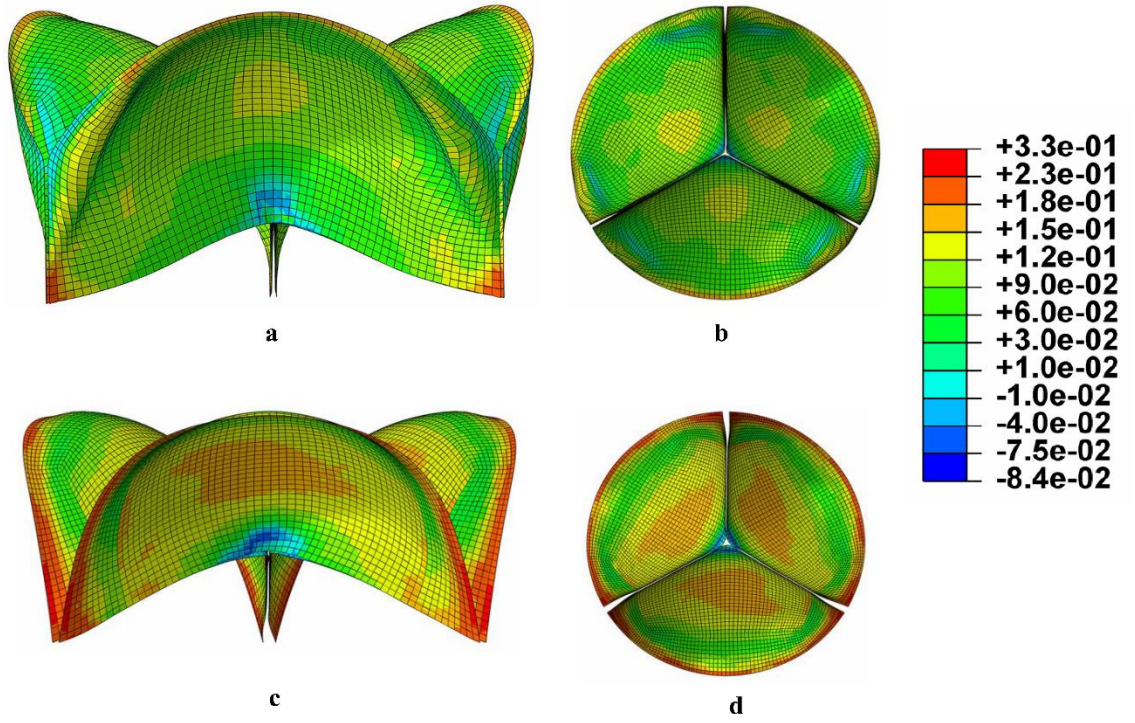

Figure 18-Maximum in-plane principal strain at peak systole, a) side view, b) bottom view Sapien 3, c) side view, d) bottom view Perimount Magna

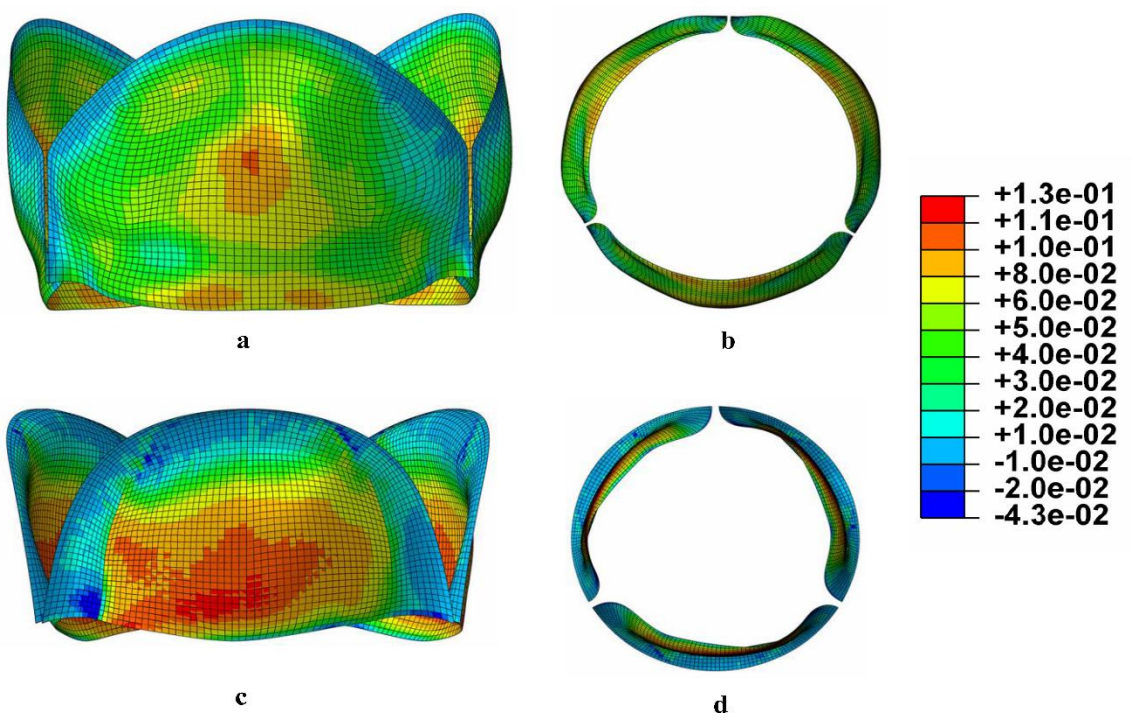

Figure 19-Maximum in-plane principal strain at peak diastole, a) side view, b) bottom view Sapien 3, c) side view, d) bottom view Perimount Magna

The von Mises stress was also plotted in systole and diastole, shown respectively in Figures 20 and 21. The peak leaflet stress value during systole for the CE PERIMOUNT Magna, and SAPIEN 3 reached to 5 and 9.2 MPa, respectively. During diastole, the peak stress value of the PERIMOUNT Magna and SAPIEN 3 leaflets reached to 0.9 and 4.5 MPa, respectively. During systole, in agreement with the maximum in plane stresses, the von Mises stress also shows high stress regions were primarily observed in the fixed boundary edges of the two bioprostheses.

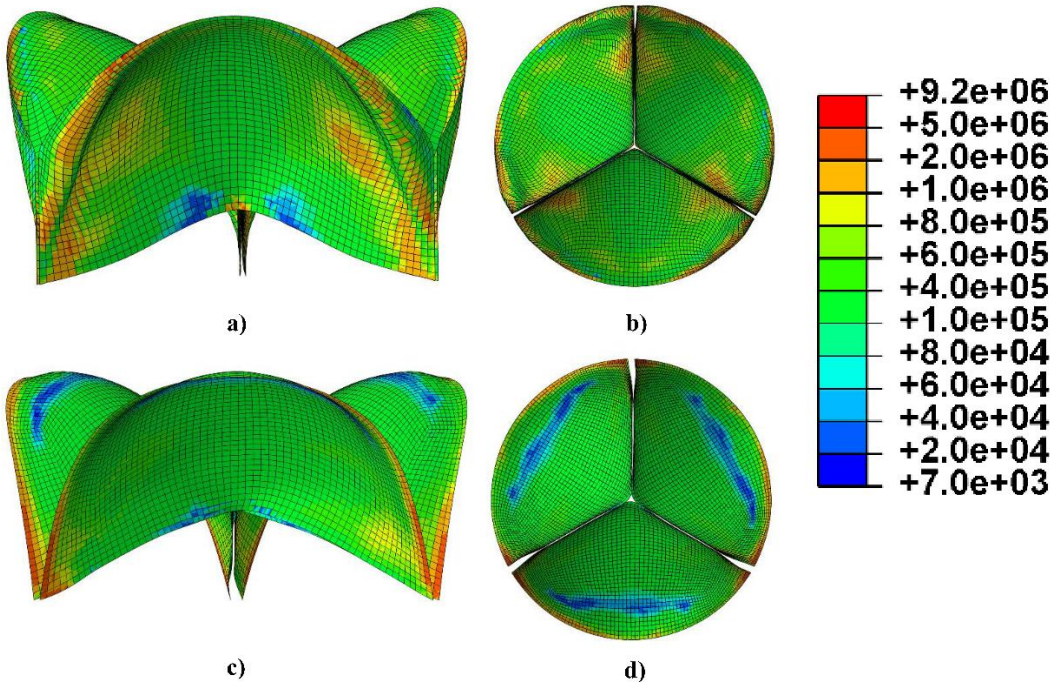

Figure 20- Von Mises stress at peak systole, a) side view, b) bottom view SAPIEN 3, c) side view, d) bottom view PERIMOUNT Magna

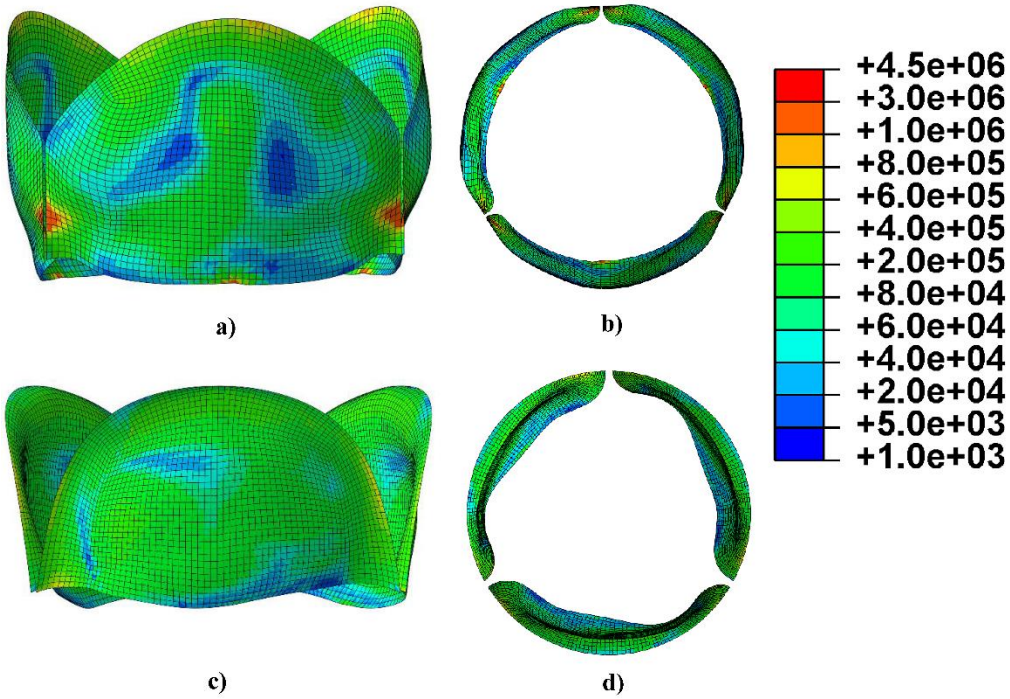

Figure 21- Von Mises stress at peak diastole, a) side view, b) bottom view SAPIEN 3, c) side view, d) bottom view PERIMOUNT Magna

In order to better demonstrate how stress values differ between the two valves under the same loading condition, the maximum in-plane principal stress histograms are presented in Figures 22 and 23 for systole and diastole, respectively. During systole, SAPIEN 3, 38.5% of elements had stress values of more than 400 kPa compared to 20.2% for the PERIMOUNT Magna. During diastole, 86.7% of the elements in PERIMOUNT Magna had a stress of up to 100 kPa in comparison to 62.8% of SAPIEN 3 elements in this range. Over 35% of SAPIEN 3 elements had stress values of over 100 kPa.

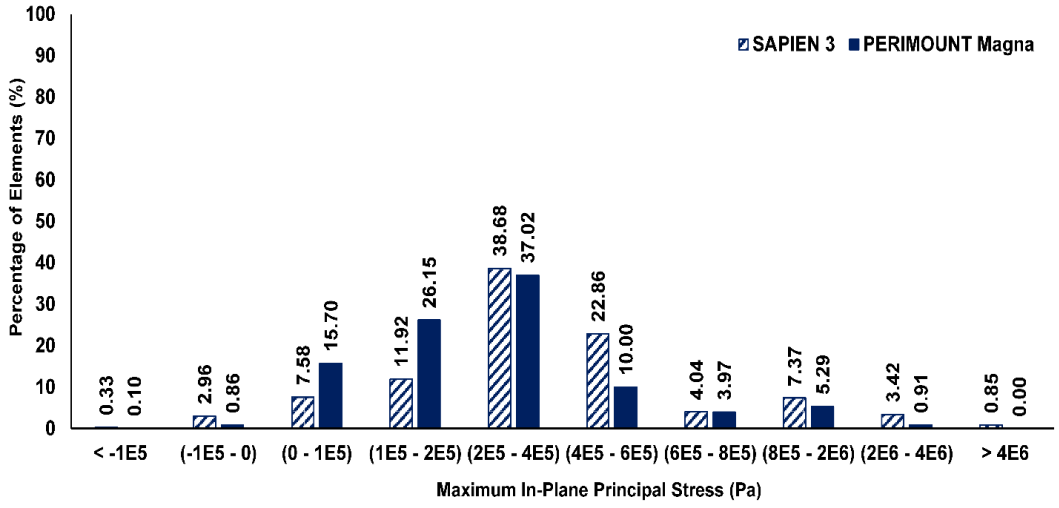

Figure 22-Distribution of maximum in-plane principal stress at peak systole at each node for each valve

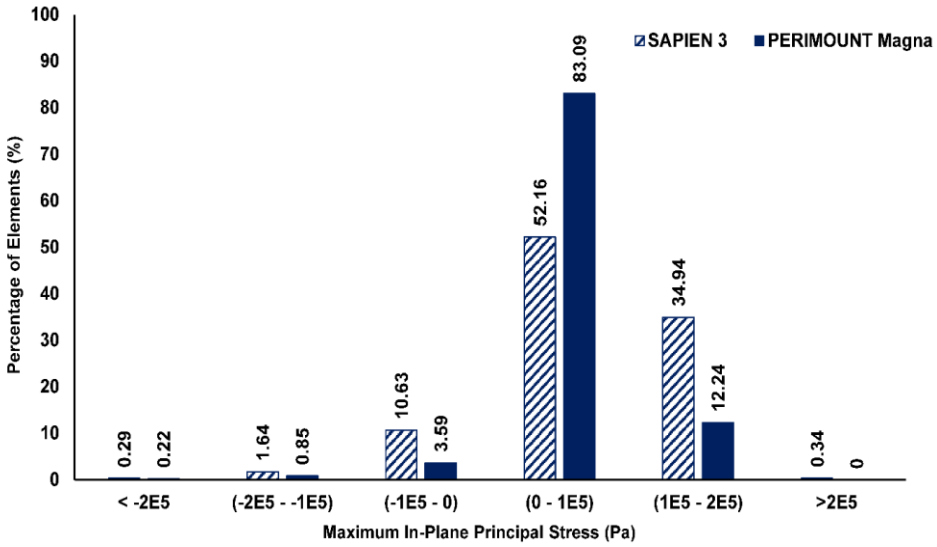

Figure 23- Distribution of maximum in-plane principal stress at peak diastole at each node for each valve

3.2.2. LV Motion Simulation

An optimization procedure was used to simulate the LV motion through identifying the hyperelastic material properties. Geometric models of the LV during the cardiac cycle were built from CT data and the apex displacement was found and tracked. The end-diastolic state was used as the reference point and the displacement relative to that was found. The initial guesses were derived from experimental stress/strain data and fitting a reduced polynomial hyperelastic material function. Reduced polynomial model parameters for the left ventricle were found with the PSO method in Isight through targeting the displacement of the apex for each coordinate x, y, z. Figure 24 a,b,c, shows the result of the optimization for coordinates x, y and z, respectively. For computational efficiency in the optimization procedure, only the apex was monitored. In addition, in Figure 24, the initial material properties' results are plotted with the optimized material parameters' results from the simulations. Looking at timing and magnitude, a clear difference is seen between them. The maximum displacement between the two simulations was 80, 85 and

42% different for x, y and z, respectively. In Figure 24 d, the displacement magnitude resulting from the optimized model and the target can be seen. The maximum target and optimized displacement is 10.24 and 10.46 mm, respectively. The optimized material parameters are listed in Table 4.

Table 4-Material parameters for reduced polynomial model for the left ventricle

	C_{10}	C_{20}	C_{30}	C_{40}	D_1	D_2	D_3	D_4
Left Ventricle	3210689	6055235	-2581107	1348871	3.5e-5	3.5e-5	5.2e-5	5.7e-5

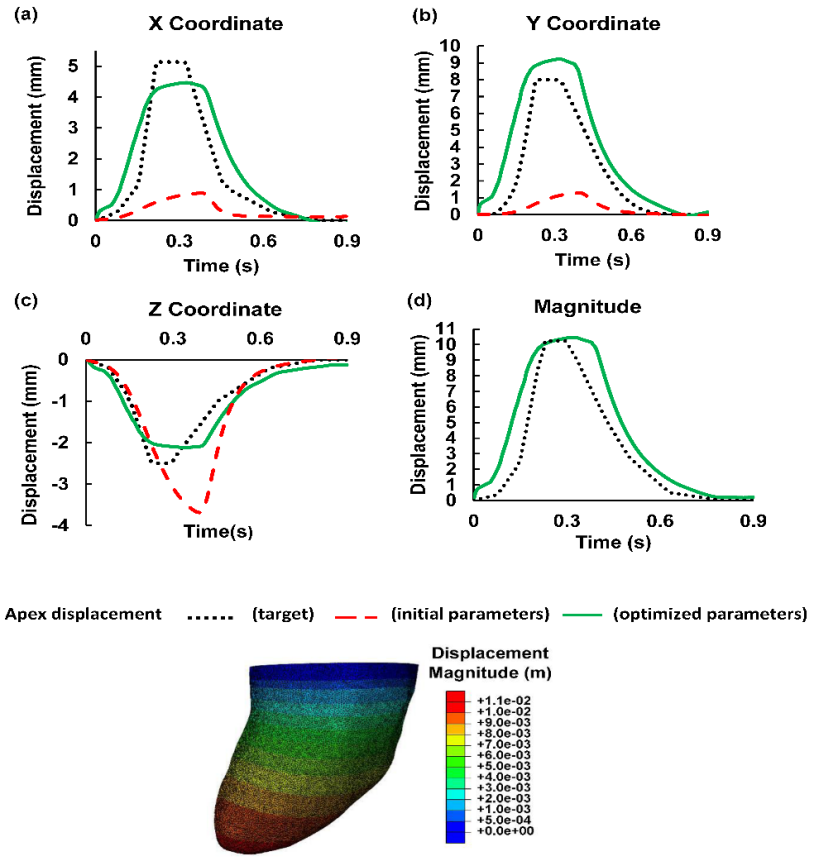

Figure 24- Optimization results for the apex displacement in each coordinate x, y and z. Each graph compares the optimized FE simulations with the target data and simulation with initial parameters

3.3. Computational Fluid Dynamics (CFD) Results

The aim of CFD modeling in this work is to initially prove the feasibility of reliable CFD modeling within the LV anatomy with steady-state simulations and in the next step, use one-way Fluid-Structure Interaction (FSI) to fully simulate the three-dimensional flow field. The FE simulations of the valve leaflets and LV are used for FSI modeling. Codes were written to create frames of the leaflet and LV movement from the FE simulations. Essentially, at every 0.2 ms, for each leaflet, a fine cloud mesh is generated based on the FE simulation, and the same for the LV which would then be read using a user-defined function (UDF). This function updates the leaflets' and LV's surface grids at each time-step with the cloud meshes. CFD models were built for the surgical, supra-annular and intra-annular transcatheter valves and the results of the steady-state simulation are presented in Figure 23. A constant inlet pressure of 1600 kPa is assumed in the simulation.

In Figure 25 a, b, c, a slice has been made in the pressure field at the tip of the leaflets exactly at the position that flow exits the valve. The valves are in the zero-pressure gradient form at the beginning of diastole when they start to open. The central jet in the intra-annular model has lower pressure compared to the surgical and supra-annular model while the surgical valve has the largest high-pressure region. Images d, e, f in Figure 25 display the same slice in the velocity field and the intra-annular jet has the highest velocity at the center. In the steady-state conditions, flow velocity and pressure are inversely related, so the results for the valves are reasonable. A clear difference between the flow velocity and pressure at the valves is seen between the intra and supra-annular position, confirming the need to study and investigate the effects of valve position on the flow and the hemodynamics. Parts g, h and i in Figure 25 show the velocity vector field within the LA

and LV. The flow jet is clearly visible within the anatomy, showing that the solution has fully converged. As the walls of the LV are stationary in the steady-state model, the flow around the walls has very low velocity (less than 0.2 m/s) but when the movement of the LV is incorporated in the model, the dynamic anatomy will directly affect the flow field.

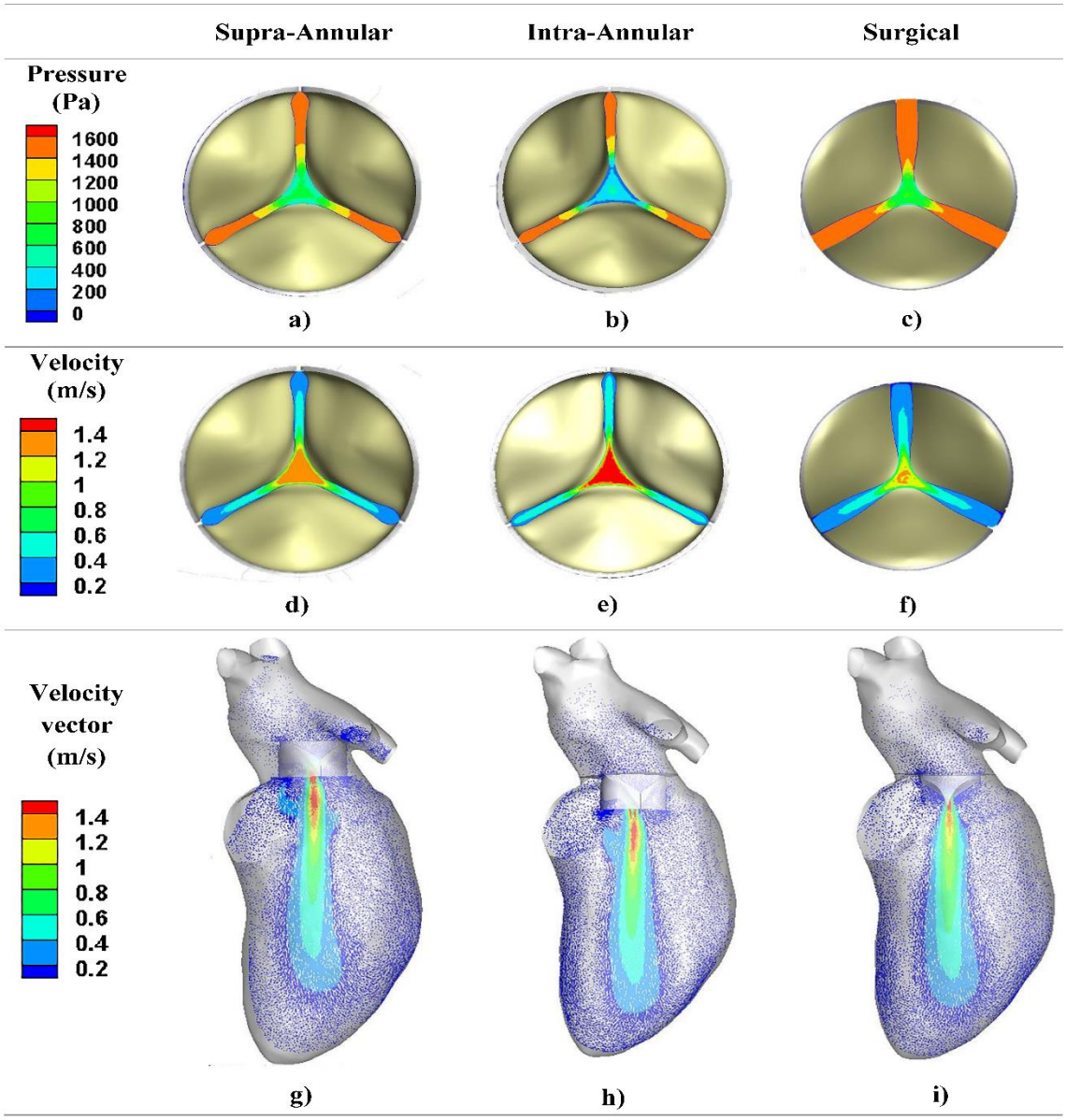

Figure 25-Steady-state CFD simulation results for supra-annular, intra-annular and surgical model

CHAPTER 4: DISCUSSION

In this study, the first aim was to predict and compare the durability of TMVR devices to surgical bioprosthetic mitral valve replacements and used a finite element modeling approach to assess stress distribution and justify its relation to durability. The leaflets' three-dimensional anisotropic mechanical properties were defined for a commercially available and well-examined surgical bioprosthesis (i.e., Carpentier Edwards PERIMOUNT Magna mitral heart valve) and a TMVR device under clinical investigation (Edwards SAPIEN M3). With a pulse duplicator system, the valves were tested under dynamic physiological loading conditions. With an optimization method, the 3D anisotropic mechanical properties of the leaflets were adjusted to become compatible with the results of the experiment. Finite element analysis with the optimized results, yielded the maximum in-plane principal stress and strain distribution for the two valves. These were compared at both systole and diastole to help predict durability.

It is essential to highlight that clinical data is the first and foremost predictor of durability, however, in the case of TMVR devices, when there is not even yet an approved device, such data do not exist. Even in the case of TAVRs, long-term data are still scarce. However, long-term durability is a critical element in choosing a suitable replacement heart valve for the mitral valve. Therefore, the only choice left is to compare with bioprosthetic valves that have relevant long-term clinical data available; in this case, surgical

bioprosthetic mitral valve replacements and to compare surgical aortic valve replacement (SAVR) and transcatheter aortic valve replacement (TAVR) and draw cautious conclusion from that. In these circumstances, the importance of computational modeling and simulation in providing insights on TMVR durability in combination with clinical data is emphasized.

Leaflets degeneration in surgical bioprosthetic valves happens through two separate, but potentially cooperating mechanisms: calcification and fatigue-induced structural deterioration. Since the TMV leaflets, similar to commercial TAV leaflets, are made from bovine or porcine pericardium tissue that has been chemically treated, it can be predicted that the same failure mechanisms apply to the structural deterioration of TMVs as well. Structural valve degeneration (SVD) happens gradually, eventually causing valve dysfunction secondary to stenosis, regurgitation, or a combination of stenosis and regurgitation (29). Although structural valve degeneration definition is varied in the literature, at 10 years, the overall SVD rate for surgical bioprostheses is less than 15% (34).

In 2014, Bourguignon et al. studied the Carpentier-Edwards PERIMOUNT pericardial bioprosthesis in the mitral position in terms of the long-term durability and reported the longest-term follow-up data with this prosthesis, with some patients at 20 years post-op. 404 consecutive patients (mean age, 68 years; 53% female) were studied. The results for SVD in this study showed the overall actuarial freedom from SVD is 83.9% ± 2.7% and 23.7% ± 6.9% at 10 and 20 years, respectively. The expected valve durability was acceptable for the long-term, with a median survival time (MST) of 16.6 years before valve deterioration. The freedom from reoperation for SVD was 86.3% ± 2.5% and 40.5% ± 8.0% at 10 and 20 years, respectively, with an MST of 19.0 years. The expected valve

durability was compared with the sample life expectancy after MVR in different age groups, concluding that at least for 90% of the cohort, the expected valve durability was greater. The study concluded the Carpentier-Edwards PERIMOUNT pericardial bioprosthesis is a dependable option for a tissue valve in the mitral position, particularly in patients>60 years old (37).

SAVR and TAVR can be compared even though clinical data beyond 5 years about long-term durability of TAVRs is currently limited. Bourguignon et al. (38) reported that recipients of CE PERIMOUNT surgical aortic valve aged 60 or younger had freedom from reoperation rates (attributable to structural valve deterioration) of 88.3 ± 2.4 and 38.1 ± 5.6% at 10 and 20 years, respectively. Dvir conducted a study on patients (n=378) with up to 10 year follow up post TAVR. These patients' valves were one of the following: Edwards Sapien XT, Cribier Edwards and Edwards Sapien. In sum, 35 SVD cases were reported: around two-thirds showed intra-prosthetic aortic regurgitation and the rest mixed disease or valvular stenosis. This study concluded an estimated SVD rate of approximately 50% at 8 years, however, due to the SVD definition in this study, the actual SVD incidence could have been overestimated (29).

The key factors related to SVD after SAVR can be split into 3 categories: those associated to the patient directly, cardiovascular risk/comorbid conditions, and valve associated factors. In the first group, in most studies, bioprosthesis durability is related to age at the time of valve implantation. At a 10-year follow-up, the SVD rate in elderly patients is commonly less than 10%, however in patients below 40, it can rise to 20% to 30%. Accelerated SVD is also related to larger body surface area, possibly due to larger hemodynamic stress and less tolerance for the adverse results of stenosis or regurgitation.

Amongst the valve related factors, the most important is the prosthesis size being too small and prosthesis-patient mismatch (PPM) which result in unusually high gradient across the valve because of the higher mechanical stress, potentially contributing to increased SVD incidences (29).

As there are few patients with long-term follow-up data, it is hard to evaluate the factors related to SVD after TAVR, leading to few cases of SVD events. However, considering that transcatheter valves are basically bioprosthetic valves, the risk factors of surgical bioprostheses can be expected to be related to post TAVR bioprosthetic deterioration, with the addition of specific considerations to the TAVR field (29). The differences between TAVR and SAVR consist of: how the native valve is dealt with at implantation (in TAVR the native cusp calcifications are left whereas in SAVR, the calcifications are removed completely), paravalvular leakage risk (due to the different TAVR implantation method in comparison to suturing techniques in surgical valve) and the need to develop low profile delivery systems for TAVR as well as crimping the valve leaflets, all of which could contribute to decreasing valve durability (29)(28). These are all issues that a TMVR device faces as well, therefore posing as potential threats against TMVR durability.

Event though TAVR prostheses are made from leaflet material that is similar to surgical bioprostheses, higher mechanical stress levels are observed on TAVR valves due to how leaflet tissue is attached to a rigid ring. In surgical valves, the stent is generally made with residual flexibility. To have a safe delivery system that poses less risks for the vascular tissue, catheter sizes are designed to be as small as possible, this feature usually

entails using thinner material for the leaflets, which in turn could be less durable in comparison to the thicker bovine pericardium used in many surgical valves (28).

Increased leaflet mechanical stress has been identified as one of the main mechanisms in the pathogenesis of SVD that cause thickened valve leaflet tissues (29). These are in accordance with the findings of our finite element modeling results. As displayed in Figure 16, the SAPIEN 3 valve has a higher maximum in-plane stress value in systole compared to the CE Perimount Magna (16 MPa in comparison to 4.75 MPa) even though this high peak is seen in few elements. Moreover, during systole, 38.5% of SAPIEN 3 elements had stress values of higher than 400 kPa compared to 20.2% of elements in PERIMOUNT Magna, verifying the clinical speculation of higher stress values with transcatheter valves. Also, in diastole, 86.7% of the elements in PERIMOUNT Magna had a stress of -100 kPa to 100 kPa in comparison to 62.8% of SAPIEN 3 elements in this range while over 35% of SAPIEN 3 elements had stress values of over 100 kPa.

This difference could arise from the thinner leaflets in the SAPIEN 3 valve (0.33 mm) compared to the 0.5 mm thick surgical valve leaflets. In order to develop delivery catheters and sheath sizes with lower profiles, the TAVR leaflets need to be made from thinner material, for example the SAPIEN 3 device currently has a 14 F delivery catheter. In accordance to these findings, TMVR devices may potentially have lower durability in comparison to their surgical counterparts. This is in agreement with the study that Martin et al. (30) led, they investigated TAV and SAV leaflet fatigue. To identify the pericardial leaflets' behavior, they built a computational soft tissue fatigue damage model and implemented cyclic loading. TAV and SAV leaflets had equal loading conditions and identical leaflet tissue properties, but higher stresses, strains, and fatigue damage were

witnessed on the TAV leaflets. They concluded that TAV durability could be significantly reduced compared to SAVs to about 7.8 years. Abbasi et al. (34) also reports higher stress values in TAV leaflets after computational simulation and speculates that the increased mechanical stress on the leaflets may clarify why the tissue degeneration is accelerated and the long-term durability is reduced.

The leaflet's computational model is only accurate if the properties that are assigned to it to simulate the bovine and porcine pericardium leaflet behavior are correct. There are reported differences in the structure and composition of pericardium leaflets, hence, it is necessary to use a three-dimensional anisotropic material model for the fixed biological tissue to correctly describe the mechanical properties of the leaflets, as done in this work. Furthermore, to correctly identify bioprostheses' failure mechanisms, it is important to inspect bioprosthetic heart valves under dynamic loading conditions.

4.1. Thrombosis

Valve thrombosis is another mechanism of failure that occurs in bioprosthetic valves (32) and this study aimed to compare the risk of thrombosis between the intra-annular and supra-annular designs, ultimately comparing the thrombosis risk to that of a surgical mitral valve replacement device. Overall, bioprosthetic valves are regarded as less thrombogenic than mechanical valves, in many cases, removing the need for long-term oral anti-coagulation therapy. Nevertheless, thromboembolic event risk is still not insignificant, especially during the first 3 months post SAVR. The incidence of valve thrombosis following SAVR is predicted as ranging from 0.03 events per 100 patient years, and a reported 15-year incidence of 0.37% to 26% (39). Another study reported that in the early post operation time after surgical bioprosthetic valve replacement, there is an increase in

risk of thromboembolic events. Early observational experience estimated the general thromboembolic risk to be around 2.3% per year post bioprosthesis implantation, with most events happening during the first 90 days.

The type of anti-coagulation therapy is also important, the Society of Thoracic Surgeons Adult Cardiac Surgery National Database stated that after bioprosthetic aortic valve replacement, embolic events have a very low rate at 90 days (0.9%), also presenting a decreased risk of death and embolic events (relative risk reduction 20% and 48%, respectively) in patients that took warfarin as well as aspirin in comparison to the aspirin-only therapy. There is no evidence of thrombosis risk in bioprosthetic mitral valve replacement, but it seems the risk of mitral bioprosthesis thrombosis is higher than what it is for bioprosthetic aortic valves (40).

Moreover, late valve thrombosis is identified as an important factor in bioprosthetic valve dysfunction in the long-term. Egbe et al. concluded from an observational study that the median time for explanting a surgical valve due to thrombosis is 24 months with 15% of cases happening later than 5 years post-op (40).

In the case of TAVR, a systematic review reported 15 THV thrombosis cases, while 14 of those were for the Edwards SAPIEN THV, with mean time to diagnosis being 9 ± 7 months. THV thrombosis seems to be a rare event: the randomized PARTNER trials and the TAVR registries did not report any cases of thrombosis. In the PARTNER EU trial, just one THV thrombosis case (0.8%) was reported out of the 130 TAVR recipients (31). During the clinical evaluation of the potential TMVR designs, the rate of THV thrombosis was rather concerning (6% to 8%) at different stages post Tendyne (Abbott Vascular, Abbott Park, Illinois), HighLife (HighLife Medical, Irvine, California), and Fortis

(Edwards Lifesciences, Irvine, California) device implantation. In the case of the Fortis THV program, Edwards Lifesciences had to stop the program because of device thrombosis issues in May 2015 (40).

As mentioned before, blood residence time (BRT) and wall shear stress are recognized as factors related to thrombus formation, providing a method of quantifying risk of thrombosis in computational simulations. Vahidkhah et al. (41) investigated the effect of transcatheter aortic valve geometric confinement on BRT over the TAV leaflets and then assessed risk of valve thrombosis post TAVR. To this end, computational models of a TAV and a surgical bioprosthesis were created to analyze how geometric confinement can affect BRT over the leaflets in cases like ViV or intra-annular positioning of TAVR. A one-way fluid-solid interaction method was developed to find the 3D flow fields. Randomly distributed particles around the leaflets were analyzed to quantify their residence time and compare BRT among the models. At different time points over the cardiac cycle, the TAV model had significantly longer BRT over the leaflets. It was concluded that when the calcified native valve or failed bioprosthesis creates a geometric confinement for the TAV, BRT increases on the TAV leaflets, potentially indicating that it is a contributing factor for valve thrombosis.

In this context, it has been shown that RT is a way of quantifying fluid stagnation in a specific location, helping to give a time frame in the process of thrombus formation (33). In this work, we initially built the groundwork to do this assessment and used steady-state simulations to verify the feasibility of finding the pressure and velocity field within the left ventricle and atrium. Even in this simplified simulation, differences in the regions and values of high pressure and velocity can be observed. The main aim is to understand if

the position of the valve within the mitral annulus makes a difference in the risk of thrombosis and compare that to a surgical valve with the hypothesis that BRT will be significantly higher on the TMV leaflets with supra-annular design compared to intra-annular design. In addition, increased regions of blood stasis will be observed around the supra-annular TMV leaflets in the left atrium. Steady-state results in Figure 23 show higher velocity and lower pressure in the main jet region in the intra-annular model in comparison with the supra-annular model, potentially indicating less stasis. However, this will need to be verified with a transient model, incorporating the leaflet and valve motion in the model and quantifying the value of BRT. The LV motion was obtained in order to build this complex CFD model and this is the main part of the future work for this research. Furthermore, a finite element analysis can be conducted to determine the influence of the leaflet thickness reduction in THVs on stress and strain distribution, and ideally find an optimum leaflet thickness that accommodates the needs of the delivery system and has similar stress distribution on the leaflets as the surgical valve.

4.2. Conclusion

In summary, in order to find the 3D anisotropic mechanical properties for bioprosthetic mitral valves while undergoing physiological loading conditions, an optimization procedure was utilized. Two different bioprosthetic heart valves that were close in terms of size were studied. After finding the optimized material parameters, an FE simulation was run for each valve to visualize the stress distribution and demonstrate leaflet deformation. In systole, at the fixed boundary edge for the bioprostheses, most high stress regions were witnessed. On the other hand, in diastole, the high stress regions were mainly seen in the commissures of the two valves. The results of the stress distribution were related

to predicting valve durability and it seems that the transcatheter valve may have lower durability due to the high stress regions observed. Computational models of the left side of the heart were built and the movement of the left ventricle during a cardiac cycle was simulated through finding optimized hyperelastic material properties. Three CFD models were built from the left heart model with the SAPIEN 3 valve placed in intra and supra-annular positions and the PERIMOUNT Magna placed intra-annularly. Steady-state simulations were run to demonstrate the feasibility of obtaining the flow field in this geometry and show initial differences between these models. Further studies include incorporating the movement of the leaflets and the left ventricle into the CFD model to quantify blood residence time and quantitatively identify the risk of thrombosis in each of these models. Patient-specific cardiac modeling could potentially help to plan procedures and find failure modes for cardiovascular interventions.

REFERENCES

1. Ole DB, Nicolo P, Shmuel B, Georg L, Francesco M, C. HH, et al. Percutaneous Transcatheter Mitral Valve Replacement. Circ Cardiovasc Interv [Internet]. 2014 Jun 1;7(3):400–9. Available from: https://doi.org/10.1161/CIRCINTERVENTIONS.114.001607
2. El Sabbagh A, Reddy YN V, Nishimura RA. Mitral Valve Regurgitation in the Contemporary Era. JACC Cardiovasc Imaging [Internet]. 2018 Apr 1;11(4):628 LP – 643. Available from: http://imaging.onlinejacc.org/content/11/4/628.abstract
3. Muller DWM, Farivar RS, Jansz P, Bae R, Walters D, Clarke A, et al. Transcatheter Mitral Valve Replacement for Patients With Symptomatic Mitral Regurgitation. J Am Coll Cardiol [Internet]. 2017 Jan 31;69(4):381 LP – 391. Available from: http://www.onlinejacc.org/content/69/4/381.abstract
4. A. NR, M. OC, O. BR, A. CB, P. EJ, A. FL, et al. 2017 AHA/ACC Focused Update of the 2014 AHA/ACC Guideline for the Management of Patients With Valvular Heart Disease: A Report of the American College of Cardiology/American Heart Association Task Force on Clinical Practice Guidelines. Circulation [Internet]. 2017 Jun 20;135(25):e1159–95. Available from: https://doi.org/10.1161/CIR.0000000000000503
5. Lazam S, Vanoverschelde J-L, Tribouilloy C, Grigioni F, Suri RM, Avierinos J-F, et al. Twenty-year outcome after mitral repair versus replacement for severe degenerative mitral regurgitation: analysis of a large, prospective, multicenter, international registry. Circulation. 2017;135(5):410–22.

6. Mick SL, Keshavamurthy S, Gillinov AM. Mitral valve repair versus replacement. Ann Cardiothorac Surg. 2015;4(3):230.
7. Seese LM, Sultan I, Gleason TG, Wang Y, Thoma F, Navid F, et al. Outcomes of Mitral Valve Repair Versus Replacement in the Elderly. Ann Thorac Surg. 2019;
8. Apostolidou E, Maslow AD, Poppas A. Primary mitral valve regurgitation: Update and review. Glob Cardiol Sci Pract. 2017;2017(1).
9. Wu AH, Aaronson KD, Bolling SF, Pagani FD, Welch K, Koelling TM. Impact of mitral valve annuloplasty on mortality risk in patients with mitral regurgitation and left ventricular systolic dysfunction. J Am Coll Cardiol. 2005;45(3):381–7.
10. Borger MA, Alam A, Murphy PM, Doenst T, David TE. Chronic ischemic mitral regurgitation: repair, replace or rethink? Ann Thorac Surg. 2006;81(3):1153–61.
11. Yoshida K, Okada K, Miyahara S, Omura A, Inoue T, Minami H, et al. Mitral valve replacement versus annuloplasty for treating severe functional mitral regurgitation. Gen Thorac Cardiovasc Surg. 2014;62(1):38–47.
12. Prendergast BD, Baumgartner H, Delgado V, Gerard O, Haude M, Himmelmann A, et al. Transcatheter heart valve interventions: where are we? Where are we going? Eur Heart J. 2019 Feb;40(5):422–40.
13. Sromicki J, Vicentini L, Miura M, Pozzoli A, Van Hemelrijck M, Taramasso M, et al. Transcatheter approaches for mitral valve regurgitation. J Vis Surgery; Vol 5 (September 2019) J Vis Surg [Internet]. 2019; Available from: http://jovs.amegroups.com/article/view/29867
14. Mack MJ, Abraham WT, Lindenfeld J, Bolling SF, Feldman TE, Grayburn PA, et al. Cardiovascular Outcomes Assessment of the MitraClip in Patients with Heart

Failure and Secondary Mitral Regurgitation: Design and rationale of the COAPT trial. Am Heart J. 2018 Nov;205:1–11.

15. Stone GW, Lindenfeld J, Abraham WT, Kar S, Lim DS, Mishell JM, et al. Transcatheter mitral-valve repair in patients with heart failure. N Engl J Med. 2018;379(24):2307–18.

16. Suradi HS, Kavinsky CJ, Hijazi ZM. Percutaneous mitral valve repair: The MitraClip device. Glob Cardiol Sci Pract. 2016 Jun;2016(2):e201617.

17. Nickenig G, Hammerstingl C, Schueler R, Topilsky Y, Grayburn PA, Vahanian A, et al. Transcatheter Mitral Annuloplasty in Chronic Functional Mitral Regurgitation. JACC Cardiovasc Interv [Internet]. 2016 Oct 10;9(19):2039 LP – 2047. Available from: http://interventions.onlinejacc.org/content/9/19/2039.abstract

18. Shapira Y. The Cardioband annuloplasty system: is it ready for prime time? Eur Heart J. 2019;40(5):473–5.

19. Maisano F, Taramasso M, Nickenig G, Hammerstingl C, Vahanian A, Messika-Zeitoun D, et al. Cardioband, a transcatheter surgical-like direct mitral valve annuloplasty system: early results of the feasibility trial. Eur Heart J. 2016 Mar;37(10):817–25.

20. Dvir D, Webb J. Mitral valve-in-valve and valve-in-ring: technical aspects and procedural outcomes. EuroIntervention. 2016;12(Y):Y93–6.

21. Cheung A, Webb JG, Barbanti M, Freeman M, Binder RK, Thompson C, et al. 5-Year Experience With Transcatheter Transapical Mitral Valve-in-Valve Implantation for Bioprosthetic Valve Dysfunction. J Am Coll Cardiol [Internet].

2013 Apr 30;61(17):1759 LP – 1766. Available from: http://www.onlinejacc.org/content/61/17/1759.abstract

22. Wilbring M, Alexiou K, Tugtekin SM, Arzt S, Ibrahim K, Matschke K, et al. Pushing the limits—further evolutions of transcatheter valve procedures in the mitral position, including valve-in-valve, valve-in-ring, and valve-in-native-ring. J Thorac Cardiovasc Surg. 2014;147(1):210–9.

23. Yoon S-H, Whisenant BK, Bleiziffer S, Delgado V, Dhoble A, Schofer N, et al. Outcomes of transcatheter mitral valve replacement for degenerated bioprostheses, failed annuloplasty rings, and mitral annular calcification. Eur Heart J [Internet]. 2018 Oct 23;40(5):441–51. Available from: https://doi.org/10.1093/eurheartj/ehy590

24. Regueiro A, Granada JF, Dagenais F, Rodés-Cabau J. Transcatheter Mitral Valve Replacement. J Am Coll Cardiol [Internet]. 2017 May 2;69(17):2175 LP – 2192. Available from: http://www.onlinejacc.org/content/69/17/2175.abstract

25. Fiorilli PN, Herrmann HC. Transcatheter Mitral Valve Replacement: Rationale and Current Status. Annu Rev Med [Internet]. 2020 Jan 27;71(1):249–61. Available from: https://doi.org/10.1146/annurev-med-051418-060028

26. El Hajj SC, Eleid MF. Transcatheter Mitral Valve Replacement: An Update on the Current Literature. Curr Treat Options Cardiovasc Med [Internet]. 2019;21(7):35. Available from: https://doi.org/10.1007/s11936-019-0734-3

27. del Val D, Ferreira-Neto AN, Wintzer-Wehekind J, Dagenais F, Paradis J, Bernier M, et al. Early experience with transcatheter mitral valve replacement: a systematic review. J Am Heart Assoc. 2019;8(17):e013332.

28. Arsalan M, Walther T. Durability of prostheses for transcatheter aortic valve implantation. Nat Rev Cardiol. 2016;13(6):360.

29. Rodriguez-Gabella T, Voisine P, Puri R, Pibarot P, Rodés-Cabau J. Aortic bioprosthetic valve durability: incidence, mechanisms, predictors, and management of surgical and transcatheter valve degeneration. J Am Coll Cardiol. 2017;70(8):1013–28.

30. Martin C, Sun W. Comparison of transcatheter aortic valve and surgical bioprosthetic valve durability: A fatigue simulation study. J Biomech. 2015 Sep;48(12):3026–34.

31. Mylotte D, Andalib A, Theriault-Lauzier P, Dorfmeister M, Girgis M, Alharbi W, et al. Transcatheter heart valve failure: a systematic review. Eur Heart J. 2015;36(21):1306–27.

32. Webb JG, Dvir D. Is transcatheter aortic valve replacement a durable therapeutic strategy? JACC: Cardiovascular Interventions; 2015.

33. Esmaily-Moghadam M, Hsia T-Y, Marsden AL. A non-discrete method for computation of residence time in fluid mechanics simulations. Phys Fluids. 2013;25(11):110802.

34. Abbasi M, Barakat MS, Dvir D, Azadani AN. A non-invasive material characterization framework for bioprosthetic heart valves. Ann Biomed Eng. 2019;47(1):97–112.

35. Firstenberg MS, Vandervoort PM, Greenberg NL, Smedira NG, McCarthy PM, Garcia MJ, et al. Noninvasive estimation of transmitral pressure drop across the normal mitral valve in humans: importance of convective and inertial forces during

left ventricular filling. J Am Coll Cardiol [Internet]. 2000 Nov 15;36(6):1942 LP – 1949. Available from: http://www.onlinejacc.org/content/36/6/1942.abstract

36. Javani S, Gordon M, Azadani AN. Biomechanical Properties and Microstructure of Heart Chambers: A Paired Comparison Study in an Ovine Model. Ann Biomed Eng [Internet]. 2016;44(11):3266–83. Available from: https://doi.org/10.1007/s10439-016-1658-7

37. Bourguignon T, Bouquiaux-Stablo A-L, Loardi C, Mirza A, Candolfi P, Marchand M, et al. Very late outcomes for mitral valve replacement with the Carpentier-Edwards pericardial bioprosthesis: 25-year follow-up of 450 implantations. J Thorac Cardiovasc Surg. 2014;148(5):2004–11.

38. Bourguignon T, El Khoury R, Candolfi P, Loardi C, Mirza A, Boulanger-Lothion J, et al. Very long-term outcomes of the Carpentier-Edwards Perimount aortic valve in patients aged 60 or younger. Ann Thorac Surg. 2015;100(3):853–9.

39. Córdoba-Soriano JG, Puri R, Amat-Santos I, Ribeiro HB, Abdul-Jawad Altisent O, del Trigo M, et al. Valve Thrombosis Following Transcatheter Aortic Valve Implantation: A Systematic Review. Rev Española Cardiol (English Ed [Internet]. 2015;68(3):198–204. Available from: http://www.sciencedirect.com/science/article/pii/S1885585714004472

40. Pagnesi M, Moroni F, Beneduce A, Giannini F, Colombo A, Weisz G, et al. Thrombotic Risk and Antithrombotic Strategies After Transcatheter Mitral Valve Replacement. JACC Cardiovasc Interv [Internet]. 2019 Dec 9;12(23):2388 LP – 2401. Available from: http://interventions.onlinejacc.org/content/12/23/2388.abstract

41. Vahidkhah K, Barakat M, Abbasi M, Javani S, Azadani PN, Tandar A, et al. Valve thrombosis following transcatheter aortic valve replacement: significance of blood stasis on the leaflets. Eur J Cardiothorac Surg. 2017 May;51(5):927–35.